Chapter 11

Metal Organic Frameworks as Emerging Photocatalysts

Ahmad Alshammari, Zheng Jiang and
Kyle E. Cordova

Additional information is available at the end of the chapter

http://dx.doi.org/10.5772/63489

Abstract

Increasing number of metal-organic frameworks (MOFs) have recently been recognised as a new generation of emerging porous photocatalysts in photocatalysis and photoelectrocatalysis, since their intrinsic coordination structure between the metal cluster and organic ligands offers MOFs great flexibility to tune their semiconducting property for enhanced light harvesting. In order to improve their performance substantially and achieve widespread application of MOF photocatalysts, it is necessary to develop effective synthesis strategies and understand their semiconducting crystal structure, photocatalytic mechanism in depth. This chapter firstly provides a brief introduction of the MOF materials; this chapter addresses the crystallinity, porosity and electronic semiconducting structures that are essential in solar energy conversion. Established and innovative syntheses strategies of MOFs are then categorised and illustrated, followed by various characterisations techniques applied to investigate their structural and semiconducting properties (band structure and charge transfer), including X-ray Diffraction XRD, small angle X-ray Diffraction SAXRD, adsorption/desorption, UV-Vis, nuclear magnetic resonance (NMR), extended fine Auger structures (EXFAS), inelastic neutron scattering (INS) spectroscopy, high-resolution transmission electron microscopy (HR)TEM and electrochemical measurements. The photocatalytic and photoelectrocatalytic application of MOFs are introduced addressing their unique photocatalytic mechanism. The perspectives of MOF photocatalysts are finally presented to encourage the future development. The content of this chapter suits the users including beginners, postgraduates and professionals.

Keywords: metal organic framework, photocatalysis, light harvesting, photocatalysis, water splitting, photocatalytic CO_2 reduction

1. Introduction

1.1. General introduction

In the late 1990s, the discovery of a new type of porous compounds has appealed great attention due to the potential these materials exhibited in advanced technological applications. These compounds, termed porous coordination polymers (PCPs) or more commonly, metal-organic frameworks (MOFs), result from the combination of two distinct disciplines, organic and inorganic chemistry, which form open frameworks. MOFs are well known to possess large surface areas due to ultrahigh porosity with the size of their pores ranging from the micro- to mesoporous regime. As shown in **Figure 1**, the structures of MOFs are composed of organic ligands (referred to as linkers) and metal clusters that serve as connecters. Due to a high degree of variability for both the inorganic and organic components, there is a large library of aesthetically pleasing structures that have been shown to be of potential use in applications such as clean energy storage (methane and hydrogen) [1], CO_2 capture and sequestration and various separation processes [2–5]. Furthermore, MOFs use in thin film devices [6, 7], biomedical imaging, light harvesting, optical luminescence [8, 9] and catalysis [10, 11] is also gaining importance.

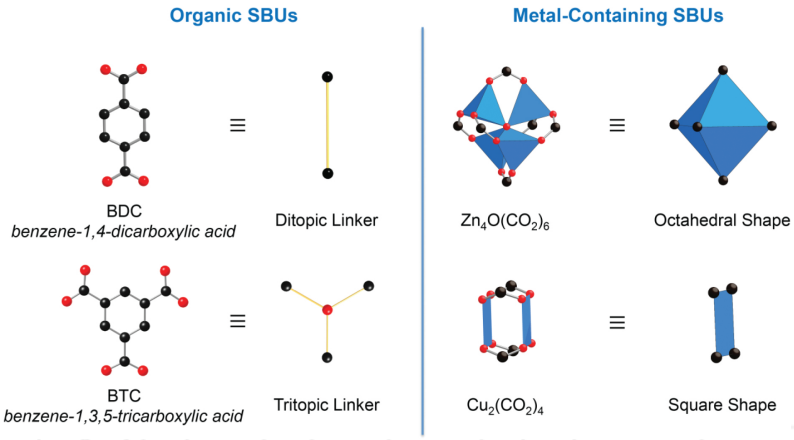

Figure 1. The chemical formula and names are provided for each MOF. Atom colours in molecular drawings: C, black; O, red; N, green; Zn, blue polyhedral; Cu, blue squares. Hydrogen atoms are omitted for clarity.

By definition, two secondary building units (SBUs) are involved in the formation of a crystalline MOF structure. The first SBU is the organic linker, which may be ditopic (having two types of coordinative functionalities), tritopic (three types) or polytopic (more than three types). The second SBU is a metal atom, a finite polyatomic inorganic cluster with two or more metal atoms, or an infinite inorganic unit such as an infinite periodic rod of metal atoms. Metal-containing SBUs are generated in situ and can be predesigned as a result of the judicious choice of reaction conditions (solvent system, temperature, molar concentration, pH). The shapes of SBUs are

http://dx.doi.org/10.5772/63489

defined by their points of extension (connectivity with organic linker SBU) and can be described as a polyhedron, polygon or infinite rod. By contrast, organic linkers are preformed to a custom shape. The aesthetic chemistry of MOFs depends on combination of given metal secondary building unit with variety of organic SBUs. In particular, the organic linker may have the same topology, but a different metric, and may yield an isoreticular series of structures with the same basic net. As organic compounds are quite flexible, it is important to properly identify all vertices and edges along with the point of extension. The components of MOFs are linked by coordination bonds and some other weak interactions (pi-electron, H-bond or Van der Waals interaction), which provide more flexibility to crystalline material and add to the usefulness of MOFs among porous materials.

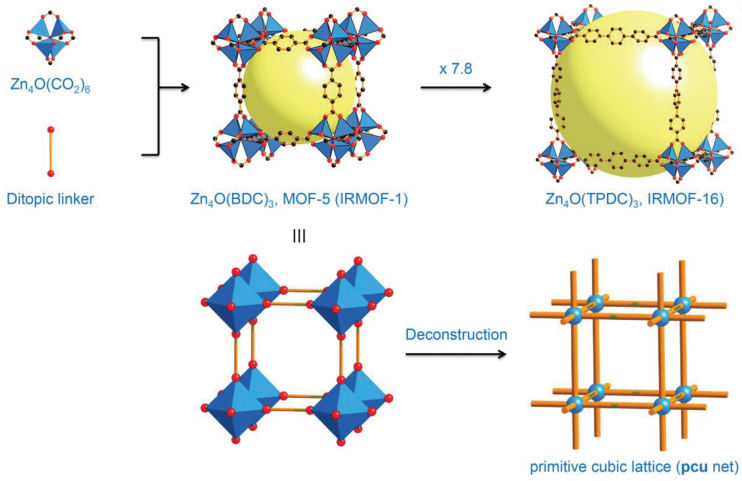

Figure 2. The chemical formula and names are provided for each MOF. Atom colours: C, black; O, red; N, green; Zn, blue polyhedral. Hydrogen atoms are omitted for clarity.

Modelling of a targeted structure with desirable properties and functions represents the eternal goal for material chemists. Therefore, first point is to comprehend the underlying geometric principles involved in MOFs crystal formation. The reverse engineering approach is used by some researchers by which crystal structure of MOFs are deconstructed into core topological nets, and helps in laying a foundation for subsequent description and designing of crystal structure of other MOFs [12]. The advancement in synthetic techniques now allows researchers to design novel and flexible porous crystalline materials by utilising the compounds and structural topologies.

1.2. Historical developments

Coordination polymers represent a group of compounds with extended entities that arise through the linking of metal ions by coordinate bonds to either organic or inorganic ligands. Coordination polymers give rise to structures which can take the form of one (1D)-, two (2D)-

or three (3D)-dimensional networks. Cu, Zn, Ag and Cd—the late transition metals—typically form such kind of network (**Figure 3**), and it was only with the advent of single-crystal X-ray diffraction (SCXRD) that coordination polymer structures could be determined. Coined as early as 1916 [13], 'coordination polymer' is not a novel concept, although it was originally not possible to verify the nature of the continuous framework in the absence of X-ray crystallography. With the discovery of the Prussian blue compounds in 1936, however, it became apparent that 3D coordination frameworks with a cyanide bridging group existed. At present, the term PCP or MOF is used to denote porous coordination polymers, given the broad use and ambiguity of the more historical term, coordination polymer [14]. According to the nature of the compound represented, distinct terminology is utilised and efforts to distinguish between their definitions can be found in the literature [15, 16], partly with respect to composition; solid compounds with considerable inorganic clusters linked by short organic ligands are distinct from those with isolated cations located within an extensive organic structure. The term MOF is typically applied to solid compounds that encompass tightly bonding, linking units of a highly crystalline and well-defined geometric composition, and which can be altered post-treatment. It should be noted that there are several key factors that can be used to explain the chemistry of these compounds. These factors are briefly discussed in following sections.

1.2.1. Coordination framework

Of the one-, two- or three-dimensional forms in which coordination polymers can be found, Hofmann and Kuspert [17] initially described layered two-dimensional structural entities, termed Hofmann compounds. The development of SCXRD method led to the elucidation of the first structure in 1949 [18]. Although such structure does not fully described until the work of Iwamoto et al. in 1967 [19], the Prussian blue complexes were discovered in 1936 and represented the first of the three-dimensional compounds.

1.2.2. Organic-inorganic hybrid materials

Given the incorporation of a CN^- ion as a bridging element within the coordination framework, the structural diversity among the established Prussian blue and Hofmann compounds remains limited. By contrast, adaptability of design and framework functionality can be attributed to the use of organic linkers. In 1959, the metal organic structure of $Cu[NC(CH_2)_4CN]_2\,NO_3$ was determined using SCXRD [20], and a broad spectrum of compounds have since been synthesised and characterised by the same means. In 1995, these types of coordination compounds were designated as coordination compounds by Yaghi et al. [21], while coordination polymers in which the nitrate ion is present in the cavity of $Cu[NC(CH_2)_4CN]_2\,NO_3$ are termed clathrates and are not regarded as porous compounds. A wide variety of clathrate type coordination compounds were described in the late 1990s.

1.2.3. Ultrahigh porosity of MOFs

The characteristic of existing as a porous material, containing an amount of small holes through which, for example, air and water can pass, is considered porosity, and it is frequently misinterpreted by researchers who use it to describe the crystallographic structures of MOFs

http://dx.doi.org/10.5772/63489

which contain guest molecules in their cavities. The description is therefore not applicable to frameworks in which the solvent molecules cannot be removed or exchanged, when describing novel MOFs which have been characterised by X-ray crystallography alone. Materials which incorporate significantly disordered, free solvent molecules which flow uninterrupted through the empty spaces of the framework can be considered as open frameworks, although the ease with which these molecules can flow out of the structure must first be determined. An evaluation of the host structure prior to and after the elimination of guest molecules is frequently used to determine the stability of MOF. In addition, the ability of a compound to retain its porosity in the absence of guest incorporation was observed in 1997 using a gas sorption procedure under ambient conditions. The novel porous compounds that MOFs represented were shown to have reversible gas storage properties and rapidly garnered a significant degree of interest. The depth of existing literature on MOFs is testament to the research which has since been carried out on these compounds, and indicates the considerable potential and new approaches that have been implemented in the design of novel and valuable MOF materials.

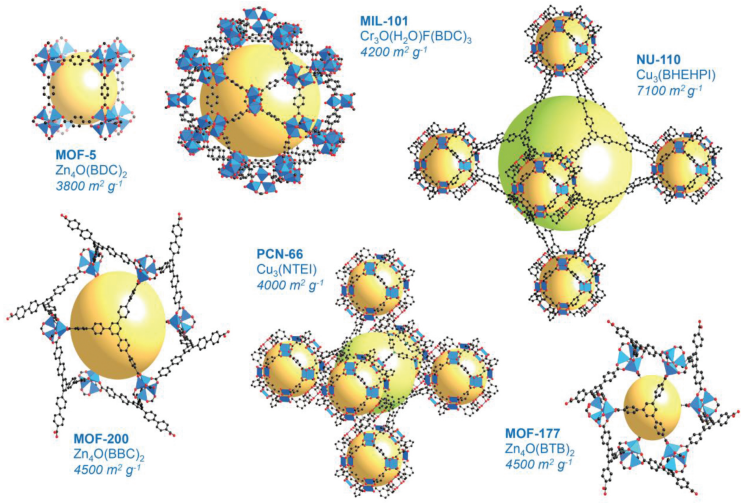

Figure 3. Crystal structure of selected MOFs with high Brunauer-Emmett-Teller (BET) surface area. The chemical formula and BET surface areas are provided for each MOF. Orange and green spheres indicate the free space in the framework. Atom colours: C, black; O, red; N, green; Zn or Cr metal, blue polyhedral; Cu, blue squares. Hydrogen atoms are omitted for clarity.

1.3. Ultrahigh surface area MOFs

Extensive surface area, the result of low density and a porous structure, is a characteristic of MOFs. A three-dimensional (cubic), porous MOF was synthesised from Zn_4O clusters linked with terephthalate [Zn_4O (terephthalate)$_3$] (MOF-5) in 1999 [22], and BET was used to calculate the surface area of the resulting compound, 3800 m^2g^{-1} [23]. The compound subsequently

formed a structural motif template for the preparation of a number of other porous compounds, a strategy which was further expanded to the design of essential frameworks. Other similar frameworks of high porosity are $[Zn_4O(btb)_2]$ (MOF-177) and $[Zn_4O(bbc)_2]$ (MOF-200) {where btb = 1,3,5-benzenetribenzoate, bbc = 4,4′,4″-[benzene-1,3,5-triyltris(benzene-4,1-diyl)]tribenzoate)}; the surface areas attributed to these compounds are 4746 and 6260 m^2g^{-1}, respectively, as determined by BET [24, 25]. Network interpenetration during the self-assembly process represents a significant limitation to structural expansion, restricting a large surface area; this issue can be circumvented using small modifications of network topology design. However, as long as the porosity of single network goes over 50%, 3D networks show more susceptibility to interpenetration, which can be eliminated, however, by using an approach in which a small side group is incorporated into a single network, thus decreasing porosity. Interpenetration can therefore be avoided through partial inhibition of the coordination network, while retaining the porosity of the final crystal. Pillared-layer-type MOF structures, for example, are largely considered non-interpenetrated as one of the three dimensions is inhibited by considerably dense layers. MOFs of adequate porosity pore size and surface can be synthesised by pillar ligands by using an appropriately layered structure format that includes coordinatively unsaturated sites. The stratification of unsaturated metal sites throughout the layer determines the pillar ligand layout. Informal pillared-layer structures (PLS), in which short pillars are used to constrain two of the three dimensions, are a class of porous MOF synthesised from porous layers with short pillars. Comparatively long bipyridyl ligands in $[M_2(bdc)_2(bpy)]$ frameworks with unsymmetrical pcu topologies, for instance, can lead to interpenetration; however, interpenetration does not take place if the pillar ligand is sufficiently small, even where the dicarboxylate ligand is overly long [26, 27]. That the 3D structure arises from layer formation in the first step and their subsequent interconnection by pillars is suggested by the term 'pillared-layer'; as the entire process (from self-assembly to crystallisation) takes place in a single pot reaction, it is therefore difficult to study. The potential exists for an individual single-layered structure to be formed through a more judicious choice of non-bridged ligand over pillared ligand. A unique incidence of the isolation of a hypothetical monolayer and pillared double layer through the preparation of pillared-layer MOFs has been reported [28].

The application of mixed ligand systems to generate porous frameworks can often be a more appropriate strategy for the design of compounds with large surface areas. Zn_4O clusters linked to a pair of separate ligands, for instance, comprise the $Zn_4O(t_2dc)(btb)_{4/3}$ (UMCM-2) (t_2dc = thieno-3,2-bithiophene-2,5-dicarboxylate) compound [29], in which micro pores were shown to be tightly dispersed at 1.4–1.6 and at 1.6–1.8 nm with a mesopore at 2.4–3.0 nm and BET surface area of 5200 m^2g^{-1}. The Zn_4O cluster is replaced with chromium in an alternative framework, and connected with a terephthalate ligand $[Cr_3F(H_2O)O(bdc)_3]$ (MIL-101) to produce a trimer composed of three chromium cations and μ_3O oxygen anions [30]. A pair of cages, 1.2 and 1.45 nm in diameter, give rise to the pores, and the compound exhibits a BET surface area of 4100 $m^2g–^1$. Increased aqueous (and other chemical) stability is observed for this structure compared with those incorporating Zn_4O clusters, and its stability and adaptability allow it to be implemented post-synthesis and for hybridisation with other materials [31].

http://dx.doi.org/10.5772/63489

The paddle-wheel-type dimetal cluster is a frequently used component of framework synthesis and incorporates a range of transition metals, giving rise to a square grid extended framework. A Cu^{+2} paddle wheel cluster has been synthesised along with 4,4′,4″-nitrilotris(benzene-4,1-diyl)tris(ethyne-2,1-diyl)triisopthalate (ntei), $[Cu(H_2O)]_3$(ntei) (PCN-66), and gave a BET surface area of 4000 m^2g^{-1} [32]. A number of alternative isostructures have also been synthesised, with the aim of generating an even greater surface area through the use of hexatopic carboxylate.

1.4. MOFs with Lewis acid frameworks

Of significant importance are frameworks featuring guest interaction sites, particularly those with unsaturated metal sites due to their application in the storage of CO_2, H_2 and other gases. HKUST-1 $[Cu_3(btc)_2.n(H_2O)]$ MOF, consisting of Cu_2 paddle wheel units connected with benzene-1,3,5-tricarboxylic acid, represents one of the earliest examples of this type of framework containing unsaturated metal sites, as shown in **Figure 4** [33]. The resulting three-dimensional network displays thermal stable materials with 1 nm pore size. Applicable in gas storage and heterogeneous catalysis, the axial sites of Cu^{2+} are accountable for incorporating guest molecules [34, 35]. Comparable motif and chromium analogues arise when metals (e.g., W, Fe) are alternatively used, displaying oxygen adsorption with type 1 isotherm at an ambient temperature at which adsorption takes place at low pressures [36–38]. Reversible chemisorption with inconsequential nitrogen uptake is similarly exhibited by the redox-active Cr centres.

In a comparable manner, a further category of frameworks with unsaturated metal cores are represented by M_2(dhtp) (H_4dhtp = 2,5-dihydroxyterephthalic acid, M = Mg, Mn, Zn, Co) [39, 40]. Mg_2(dhtp), one member of this category, displays a significant uptake of CO_2 (almost 35.2

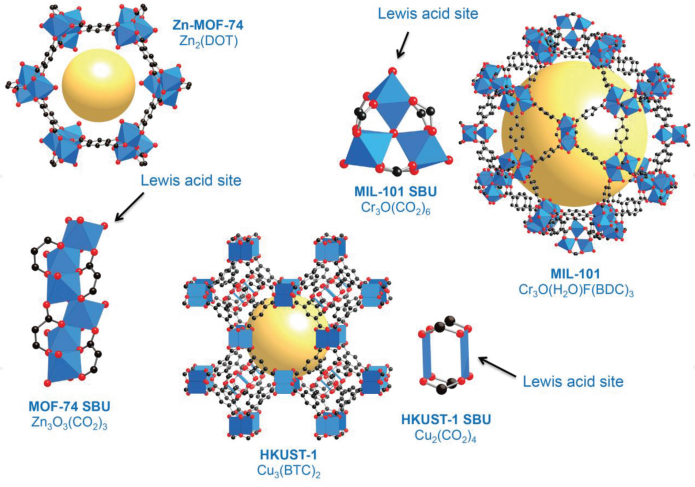

Figure 4. Orange spheres indicate the free space in the framework. Atom colours: C, black; O, red; N, green; Zn or Cr metal, blue polyhedral; Cu, blue squares. Hydrogen atoms are omitted for clarity.

wt%, at 1 atm and 298 K) which is attributable to the strong interaction of oxygen with metal and the low weight of the framework [41]. Exhibiting a high degree of hydrophilicity and acceptable stability, the compound is a biocompatible material and can be used to trap not only CO_2 but also other gases such as NO [42].

Applicable as a catalyst and featuring unsaturated Cr^{+3} centres, $[Cr_3F(H_2O)O(bdc)_3]$ (MIL-101), the aforementioned MOF with high porosity, has the additive benefit of large pores which facilitate effective substrate diffusion during heterogeneous catalysis [43, 44]. Following complete expulsion of the coordinating guest, the unsaturated sites are replenished and an organic linker can be further included into the unsaturated metal cores [45]. The addition of strong Lewis sites to the framework is challenging when using a self-assembly approach, although high design flexibility may provide a template for multifunctional catalysts. The implementation of post-synthetic procedures is a valuable approach for incorporating unsaturated metal sites into the framework and may also be applied to the addition of functional groups to MOFs with satisfactory outcomes for catalysis or other purposes.

1.5. Soft porous MOFs with flexible framework

With respect to structural flexibility and dynamic attributes, the soft properties of MOFs are described in the existing literature to date. Where porous compounds forfeit their porous structure following guest expulsion, porous compounds which can incorporate guest material can nonetheless be determined. These compounds are classed as soft porous materials and display some important and unique characteristics [46–48], although their adsorption isotherm is frequently variable as a result of dynamic guest accommodation properties and therefore cannot be determined using the standard International Union of Pure and Applied Chemistry (IUPAC) classification [49]. A gate-opening behaviour, in case no initial uptake of guest molecules to a specific concentration is observed, is a feature of soft porous materials; upon attaining the threshold concentration, a sudden increase in adsorption behaviour is observed which is linked with the structural change from the non-porous to the porous phase. Compound softness is extremely sensitive to the gas species to be incorporated, a characteristic of value in gas separation. 2D materials can usually be transformed in a straightforward manner upon guest accommodation, and a distinguishing composition of soft porous materials featuring gate type sorption has been reported [50]. 2D materials with interdigitated layers are specifically relevant, given that interlayer relationships can be modified by careful adjustment of the groups to be interdigitated. Upon guest incorporation, numerous chemical compounds displaying this behaviour have been described, all featuring a characteristic transformation [51].

A category of coordination polymers with interdigitated structures which incorporate zinc $[Zn(bpy)(C_5H_6O_4)]$ (CID-1) and further illustrate the nature of these materials have been described [52, 53]. V-shaped dicarboxylate, 4,4′-bipyridyl and dipositive metal units comprise the 2D layer, and the gate-type sorption function is significantly modulated by the effect of interactions between various carboxylate ligands and the subsequent layers. CO_2 gas, the partitioning of which from the CO_2-CH_4 mixture is partly facilitated by the flexible nature of

http://dx.doi.org/10.5772/63489

the structure, can be easily emitted with low energy consumption, given that the separation of CO_2 requires only structural flexibility without the need for strong interactions. The process can therefore be considered to differ significantly from standard separation strategies that use strong binding energies.

This flexibility is not only being attributable to the 2D structures as 3D porous frameworks also feature intrinsic flexibility. [Al(bdc)(OH)] (MIL-53), displaying diamond shaped 1D channels, is an example of this type of framework [54]. Al-OH-Al units are used to link one of the axes, and the Al-O-Al bond angle can be modified by guest sorption. Material softness can be attributed to elements such as rotatable single bonds, bond reorientation and weak supramolecular interactions, and a significant effect on the general properties of the porous structure can arise from even a minor variation in bond angle/distance. Flexible frameworks also discard a long range ordered arrangement so that amorphous or quasi amorphous phases develop. Al(bdc-OH)x exhibits selective adsorption of p-xylene isomers and in drug delivery applications as a result of its guest-mediated flexibility [55, 56]. Rearrangement of network topologies and orientation in local bonds contribute in parallel to the flexibility of MOFs. Interpenetrated frameworks, with respect to network rearrangement, can sometimes display soft material properties as a result of adjacent network rearrangement. $[Zn_2(bdc)_2(bpy)]$ (MOF-508), which is found in both open and closed forms according to the relative network position, is an example of a compound with twofold symmetry [57]. The type of guest molecule determines the change from the closed to the open form, a trait of value in the separation of pentane and hexane branched and linear isomers. The characterisation of guest molecules can be facilitated by the sensitivity displayed by this type of flexible MOF, the application of which in industrial gas separation is the subject of additional research.

2. Potential applications of MOFs

The highly periodic and crystalline nature of MOFs can be readily revealed by their crystal structures, a useful evaluation when determining structure-property relationships. When incorporating guest molecules into the framework, however, their subsequent removal may lead to structural collapse as a result of weak coordination bonds, unlike the stronger covalent bonds observed in standard adsorbent compounds. MOF structure becomes distorted upon exposure to heat and guest removal, suggesting that the compound do not exhibit true crystallinity. Given that a rigid, highly thermostable framework is considered of functional value [58], several MOFs with stability up to 300 or 400°C (and even 500°C) have been developed, rendering them suitable for the majority of applications. Although heat resistant, these compounds have other limitations including chemical instability in the presence of moisture, as exhibited by carboxylate-based MOFs. Azolate-based frameworks (metal-azolate framework, MAFs), on the other hand, display suitably strong coordination bonding between the metal-azolate system and therefore show a greater degree of stability when exposed to heat or chemicals. MOFs can thus be considered suitable for novel practical applications as a result of these varied and singular structural characteristics.

2.1. Gas storage

The extensive surface area and significantly greater pore volume, compared with activated carbon, zeolites and other standard adsorbents, are notable features of MOFs that contribute to their value in gas storage. An adaptable and modifiable synthesis process in which various permutations of metal nodes and organic linkers give rise to multiple original compounds with affinities specific to different gases. A particularly high incorporation of gas has been observed in MOFs, which resulted in very large BET surface areas (up to 6000 m^2/g) that have been formulated to date [59]. As a result of dispersive and repulsive interactions between gas molecules and framework atoms, MOFs can exhibit surface gas sorption. Modulation of the interactions of gas molecules with the surface of MOFs with the intent of optimising gas storage is the focus of much research, and can be achieved by incorporating unsaturated metal sites into the nodes [60–62], by catenation of the framework [63–67] or by substitution of different functional groups of the organic linkers [68, 69]. It is only when the adsorption capacity is significantly greater than that of the empty container that the adsorbent is of value, and several MOFs that have a large pore volume adsorb substantial quantities of nitrogen at 77 K. Given that a greater volume of liquid nitrogen can be kept in empty container at the same temperature, these compounds are not of particular use. MOFs can also effectively adsorb CO_2, although the readiness of CO_2 to liquefy also renders this property of little value. The storage of gases such as hydrogen, methane and acetylene, which are hard to be compressed, is thus a suitable application for MOFs.

2.2. Hydrogen storage

Given its high gravimetric energy density, low toxicity and formation of water upon oxidation, hydrogen is considered a valuable, more clean and high-energy fuel. Its extremely low boiling point and volumetric density of just 0.089 kg/m^3, however, present major challenges to its storage. Although multiple approaches to this have been evaluated, none have proved suitable for practical purposes. Chemical absorption, one frequently implemented approach, is capable of high storage capacity; the process is not reversible, however, meaning that hydrogen release is significantly reduced. Porous MOFs, on the other hand, absorb hydrogen strongly [70, 71], and some with ultrahigh surface area and porosity are capable of approaching the requirement of the department of energy (DOE) in the USA for H_2 storage which about 6.5 wt% and 45 g/L. However, as the enthalpy for physical adsorption is insufficiently low, these requirements are attainable only at relatively low temperatures (e.g., 77 K). Modulation of pore size, a key determinant of affinity, is one of several methods to increase the adsorption affinity of MOFs, despite the incompatibility of extremely small pore sizes with extensive surface areas in practical use. Application of unsaturated metal to the pore surfaces can significantly increase physical adsorption, but framework density is subsequently affected by such an increase in metal concentration.

2.3. Methane storage

An advantage of methane, an important fuel source and major component of natural gas, is that it burns in more clean manner compared to gasoline and exhibits a greater H_2/C ratio

http://dx.doi.org/10.5772/63489

compared to other non-renewable hydrocarbon [72]. Gasoline, however, has a volumetric energy density three times that of methane. Compounds capable of increasing the volumetric density of methane may therefore be beneficial in the transport of natural gas. Given its significantly higher boiling point compared with hydrogen, methane is readily absorbed by porous materials. By establishing a storage specification of 180 v/v (which certain highly porous MOFs are capable of attaining), the DOE encourages the research activities for developing new and unique materials for gas storage, particularly methane. An efficacious and porous framework, Cu_2(adip), adip =5,50-(9,10-anthracenediyl)di-isophthalate, which is known as PCN-14, with a large Langmuir surface area approaching 2100 m^2g^{-1} was first introduced by Zhou et al. [73]. A CH_4 uptake of 230 v/v at 290 K and 35 bar is achieved by this network as a result of its 0.8 cm^3g^{-1} pore volume and nanocage-type pores, as well as large aromatic rings on the pore surface. In addition to uptake, storage can be considered as the elimination or expulsion of gas, despite the primary research focus of raising the adsorption affinity of MOFs in order to optimise gas storage capacity. Adsorption levels measured between a pair of temperature or pressure coordinates, instead of at a single point, can be considered the effective storage capacity, and desorption can present challenges under conditions of elevated adsorption enthalpy. The peak storage value is known to occur at an adsorption enthalpy of 15.1 kJ mol^{-1} [74], under standard type-1 hydrogen isotherm storage conditions between 1.5 and 35 bar and 298 K. The sudden decline in type-1 isotherms observed under low pressure conditions correlates to a significant level of adsorbate which cannot be desorbed. A high uptake of 48.3 gL^{-1} was observed for highly porous MOF-177, at 1.5 bar as well as not only at 70 atm, suggesting an effective storage capacity of 40 gL^{-1} [75].

2.4. Acetylene storage

Given its widespread application as an essential until in organic chemistry, the global production of acetylene approaches half a million tonnes annually [76]. Its transportation presents challenges, however, given its considerable instability and inability to be compressed above an explosive threshold of 2 bar, unlike hydrogen and methane. Furthermore, products such as benzene or vinylacetylene can be formed at higher concentrations of acetylene. A need therefore exists to formulate a comparably high surface area material without the corresponding high pressure requirements, and research into huge BET surface area adsorbents for low pressure acetylene desorption has thus been reported in the literature [77–79]. Zeolites, MOFs and other microporous compounds absorb relatively large amounts of acetylene, although their excessive desorption affinity limits desorption to below 1 bar. Type III and V isotherms exhibit superior storage capacity than type I, which typically retains an excess of guest molecules; these isotherms display a low adsorption capacity and affinity, however. By designing an appropriate pore surface structure and flexible framework, MOFs can be developed which exhibit lower affinity and optimum uptake difference at working temperatures [78]. For example, Zhang and Chen [78] reported that a metal azolate framework shows an increase of acetylene volumetric storage at 1 atm using 40-fold, while an analogue of MOF-505 exhibited exceptional storage capacity under ambient conditions [79]. Enhancing the capacity storage of acetylene (230 v/v and 1 atm) for a Co analogue was demonstrated by Xiang et al., who synthesised a series of isostructural [M_2(DHTP)] MOFs, where M = Co, Mn, Mg or

Zn and DHTP = 2,5-dihydroxyterephthalate, compounds known as M-MOF-74 [80], CPO-27-M [81] and M/DOBC [41] using open metal sites [77]. Within the same MOF, the authors contrasted the acetylene binding energies at Mg, Mn, Zn and Co metal sites and reported that acetylene exhibited the greatest affinity for the Co analogue, with a binding energy of 18.5 $kJmol^{-1}$ that followed by 17.3, 16.9 and 16.5 $kJmol^{-1}$, respectively.

3. Synthesis of MOFs

When implementing the range of strategies that can be used to generate MOFs, specific parameters must be taken into account in parallel with the geometric specifications of MOF design. One such parameter is building block integrity, which must not be compromised. To date, emphasis has been placed on developing new and original organic connections and the conditions most appropriate for sustaining group functionality and conformation, while remaining sufficiently reactive to form metal-organic bonds. Conditions must facilitate the conservation of linking units for synthesis which requires the in situ preparation of SBU, a process which can be achieved through precipitation of the product from the solution. This potential drawback can be circumvented by implementing a solvothermal strategy, given that solubility is an essential property of SBU. As the preparation of single crystals appropriate for single crystal analysis was originally the primary objective of MOF synthesis, earlier studies were therefore exploratory prior to the development of an adequate knowledge base. MOF design is typically influenced by intermolecular forces that limit predictability, as well as synthetic conditions which warrant optimisation to allow building units to be amassed in a specific manner. Minor adjustments in pH, solvent polarity, concentration or temperature have widely been associated with inferior quality crystals and even the formation of an entirely different phase. Crystals of optimum quality and maximum yield can be achieved under a low energy expenditure and acceptable time frame, with adequate comprehension of the optimised conditions.

3.1. Solvothermal synthesis

MOF can be successfully prepared using solvothermal and hydrothermal strategies, uncomplicated and well-established approaches which were adapted from zeolite synthesis and therefore remain in use today [82]. The process usually requires metal salt and carboxylic acid to be combined in an appropriate solvent, stoppered and incubated until the reaction is complete, after which the product crystallises out from the original solution. Given its extensive range of solubility, high boiling point and ability to serve as a weak base to deprotonate carboxylic acid, DMF is frequently designated the most suitable solvent for this purpose. Some benefits of using the solvothermal method over other, less simple approaches include the production of large crystals, ready scalability of synthesis and the capacity to use high throughput methods, and reaction efficiency can also be improved using microwave applications. However, this approach is limited by low product yield, extensive reaction times, and the need for high temperatures and toxic solvents such as Dimethylformamide (DMF) [83].

3.2. Microwave assisted synthesis

This approach harnesses the interaction of electromagnetic waves with charged molecules of polar solvent molecules which hence facilitating a quicker reaction rate as well as improved particle size reduction, phase selectivity and controlling the morphology. The synthesis of MIL-101(Fe) was described by Lin et al. using DMF at 150°C, and a yield of 20% with particle size approaching 200 nm was reported [84]. Cr-MIL-101, an additional MOF of interest, has also been prepared using microwave heating at 210°C [85]. By raising the concentration of water or the pH value, crystal size can be reduced, as illustrated by research into reaction parameters which demonstrated that uniform crystals of 50 nm can be synthesised efficiently when optimised conditions are used. Using an analogous approach, Cr-MIL-101 of 100 nm in size was synthesised by Zhao et al. and applied to the adsorption of benzene up to 16.5 mmolg $^{-1}$ at 288 K and 56 mbar [86]. Microwave helps to synthesise the materials at 95°C, and a reduced duration of 9 min has also been used to produce MOF-5 [87]; the p-XRD pattern of which, apart from a smaller size of 5–25 μm, was similar to that produced using a solvothermal approach (where a size of almost 500 μm is typically obtained). Increased research focus on Zr-based MOFs is apparent as a result of their significant thermal and chemical stability [88], a property which can be attributed to strong coordination interactions of high charge density zirconium (Zr(IV)) ions with oxygen component of organic linkers. A microwave-assisted solvothermal approach to prepare phase pure MIL-140 was described by Liang et al. in 2013 [89], resulting in a superior compound with reduced preparation time than that required for conventional electric heating approaches. The generation of highly crystalline, prototype, octahedral-shaped crystals of UiO-66 with 1.26 wt.% H_2 storage capacity was developed by Ren et al. using a process which required as little as 5 min to complete [90].

3.3. Vapour diffusion

A relatively straightforward approach for the preparation of MOF is vapour diffusion, requiring salt and acid ligand to be dissolved in a solvent like DMF and transferred to an open vessel surrounded by a volatile base such as triethylamine. This volatile base gradually diffuses into the reaction mixture where MOF synthesis is promoted by acid deprotonation, which causes the concentration of conjugate base of acidic ligand to increase. Given the prolonged diffusion rate and reaction time of this process, large crystals can be produced at ambient temperatures [91]. This approach was adopted by Wu et al. to produce [Pb(1,4-NDC)(DMF)] [91] by dissolving $Pb(NO_3)_2$ and H_2-1,4-NDC (naphthalene dicarboxylate) in DMF in one vessel, situated within a second vessel in which triethylamine was also dissolved in DMF. Steady growth of MOF crystals resulted from the prolonged diffusion of triethylamine from the outer to the inner container.

3.4. Gel crystallisation

Gel crystallisation, an advantageous approach to the synthesis of MOF, requires a gelling agent to be added to the reaction mixture, thus decreasing the rate of diffusion and subsequently the rate of framework formation by increasing the viscosity of the solution. Using this strategy, Tuikka et al. [92] synthesised $[Ba_2(O_3P(CH_2)_3PO_3)]._3H_2O$ MOF by initially dissolving the metal

salt, barium(II) chloride, in water and a gelling agent (tetramethoxysilane). The mixture was thoroughly mixed before being used to produce a gel, upon which layers of ethanediphosphonic acid in aqueous solution were prepared and incubated for a period of 3 weeks. Although this process requires a considerable amount of time, with additional separation stages necessary to purify the product, crystals of a reasonably large size can be produced using this method.

3.5. Solventless synthesis

MOF preparation requires the use of relatively toxic solvents, an important issue which is the focus of several studies. A suitable approach is the use of solventless synthesis which, as the name implies, reduces solvent toxicity by eliminating it from reaction. Mechanosynthesis (or milling) represents a rapid, scalable and non-toxic strategy for producing MOFs, as reported by James et al. [93], in which ball bearings are placed into a stainless steel vessel with the reagents and a stoichiometric quantity of solvent. MOF synthesis proceeds following complete closure of the vessel and pulverisation of the reagents by thorough mixing. Given the nano- to microcrystalline nature of the resulting product, rapidly synthesised at room temperature (a standard liquid-assisted grinding reaction running at 30 Hz requires only 20 min), this approach can be considered relatively efficient [93].

3.6. Sonochemical

A straightforward and productive approach, the sonochemical synthesis of MOFs can be performed by subjecting the reaction mixture to ultrasound waves at an intensity of 20 kHz to 10 MHz. Some benefits of this strategy include the lack of extra heat needed, a rapid reaction time and the generation of a monodispersed crystalline product, which is of value in membrane coating applications [94, 95]. Given that crystals are instantly produced within local solvent cavity regions of short life time (ms) and size in the range of ten of microns, sonochemical synthesis can be considered an appropriate method for the generation of nanoscale crystals [96]. Under a phenomenon termed cavitation, a region within which bubbles develop expands and collapses, the effective temperature can rise to as much as 5000 K with 1000 bar pressure [96]. Several examples of MOFs synthesised by a sonochemical approach at room temperature are MOF-5, MOF-177 and HKUST-1 [97, 98]. Fard et al. showed the synthesis of a 2D MOF $[Pb_2(N_3)(NO_3)L_2]$, (L = 8-hydroxy quinolate) in aqueous solution using a sonochemical strategy, after which the nanocrystals produced can be calcinated to 400 °C to generate nanosized PbO [99].

3.7. Electrochemical synthesis

Although unsuitable for implementation on an industrial scale, electrochemical synthesis offers a different approach to the sonochemical process without the need for an external heat source. This strategy also does not require a base for deprotonation of acid, given that ions are produced by the reagents in solution. MOF membranes of high standard can be synthesised using this approach due to the well-dispersed coverage of scaffold it entails. Using direct nucleation on an anode surface with an EtOH-H_2O solution and a copper mesh, which reacted

with anions and thus did not require metal salt with calculable linker depletion, the synthesis of HKUST-1 was described by Joaristi et al. [100]. Process continuity and speed at ambient temperature are advantages of the direct nucleation approach, which is limited however by the disassociation of copper from the anodic scaffold and loss of film at the scaffold extremities [100]. Implementing an electrochemical process whereby 1,3,5-benzenetricarboxylic acid (H_3BTC) was dissolved in a 2:1 mix of ethanol and Milli-Q water under high temperature and pressure in an electrochemical cell, MIL-100(Fe) was first produced by Campagnol et al. in 2013 [101]. Both in the form of crystals and as deposits on pure iron substrates, MIL-100(Fe) was synthesised at temperatures ranging between 110 and 190°C and current densities of 2–20 mAm cm^{-2} using an Fe anode. With respect to HKUST-1, the HT-HP cell was shown to be applicable for the alteration of MOF crystal morphology. Research by Stassen et al. [102], in which synthesis was initiated by heating a solution of $BDC:HNO_3:H_2O:AA:DMF$ = 1:2:4:5/10/50:130 to 383 K, resulted in UiO-66 anodic/cathodic electrochemical film deposition on zirconium foil through the application of 80 mA at 383 K. Although a benefit of cathodic deposition includes broad substrate flexibility, better MOF adhesion on zirconium substrate was reported for anodic deposition.

4. MOFs as photocatalysts

With ever-increasing demands of energy and with fossil fuels becoming ever more diminished, solar energy represents an attractive alternative solution and a large body of research describes the harnessing and sequestering of energy from the sun. Several approaches to transform and store solar energy as chemical bonds have been proposed, including photochemical procedures such as the reduction of CO_2 and H_2O splitting. The inherent ability of plants to trap sunlight and transform water and CO_2 to carbohydrates (a process termed photosynthesis) is the source of much inspiration for researchers in the field. The development of techniques to facilitate photochemical transformation has also been the subject of significant focus. Despite certain materials exhibiting the ability to split water by harnessing UV light [103–106], some restrictions on the use of the solar spectrum exist. It nonetheless remains of primary importance to formulate a stable, efficient and cost-effective approach that can convert solar energy by capitalising on the maximum solar spectrum.

The absorption of light by certain photoactive organic molecules causes them to undergo changes which normally cannot be facilitated under standard thermally activated conditions. Given that the large part of the spectrum is not used by organic compounds, which only absorb UV photons, their efficiency is suboptimal. Limitations related to solar spectrum absorption can be mitigated by the use of molecular dyes which can absorb low energy photons, giving rise to new photocatalytic reactions under visible light [107–111]. Three stages comprise the conversion of solar energy into useful chemical energy: the generation of charge-separated excited states by using a photosensitiser to absorb sunlight, the creation of redox equivalent and subsequent transfer to reactive sites and the presence of oxidation and reduction half reactions at catalytic centres. With the objective of merging photosensitiser and catalytic components into covalent bonded dimers, supramolecular structures or polymers [112–114],

several types of compounds have been generated; this approach has a high degree of complexity, however, in that the process is laborious and requires many steps, thus limiting it applicability.

As a novel category of organic-inorganic hybrid supramolecular structures, MOFs can function as photocatalysts for the main reason that they incorporate photosensitiser and catalytic functionality within one structure. The aforementioned three stages of photocatalysis are thus facilitated within one solid compound [115]. Through substitution of the standard photocatalyst which typically includes heavy metals, photoactive MOFs can function as superior photocatalysts by minimising contamination and can readily be recovered and reused due to their solid form, thus conferring fiscal benefits.

4.1. Hydrogen generation by MOFs

Given their significant potential for harvesting solar energy, research efforts in the past 10 years have been devoted to the production of compounds that can serve as photocatalysts for the production of H_2 from H_2O, with several candidates having been described to this end. Catalytic activity has thus been reported for UiO-66, a simple MOF [116] with a photocatalytic water-splitting capacity which has been verified in a water-methanol system. The photocatalytic activity of this compound was shown to be increased by the introduction of platinum nanoparticles as a co-catalyst [117], and the location of an amino group within the MOF structure was shown to create intense absorption (between 300 and 400 nm) with a marginal increase in catalytic activity [118]. Lin et al. described an MOF for hydrogen evolution comprising molecular phosphor as a structural unit in addition to platinum nanoparticles [119]. Given the reported success of using iridium-based photosensitisers, an iridium-based MOF was synthesised using bis(4-phenyl-2-pyridine)(5,5′-dicarboxylate-2,2′-bipyridine)-Ir(III) chloride or bis(4-phenyl-2-pyridine)(5,5′-di(4-phenylcarboxylate)-2,2′-bipyridine)-iridium(III) chloride structural units with $Zr_6(O)_4(OH)_4$ SBUs. The resulting MOF exhibited superior stability in aqueous solution, and Pt nanoparticles were incorporated within the MOF spaces using in situ photoreduction of the Pt precursor. This type of MOF exhibits extremely high photocatalytic activity, probably attributable to readiness of electrons to transfer between platinum nanoparticles and Ir complexes.

4.2. Photocatalytic reduction of carbon dioxide on MOFs

Given its capacity for CO_2 reduction from the environment without the need to utilise solar energy, significant research focus has been turned to catalytic reduction of carbon dioxide. Several compounds such as semiconductors and metal-based zeolites have been recently described for the photocatalytic reduction of CO_2 [120–123]. Lin et al. reported in 2011 the production of an MOF catalyst $Zr_6(\mu_3\text{-}O)_4(\mu_3\text{-}OH)_4(bpdc)_{5.83}(L_8)_{0.17}$ (where bpdc = 5,5′-biphenyldicarboxylate and H_2L_8 = $Re(CO)_3$(5,5′-dcbpy)Cl) through the introduction of $Re(CO)_3$(5,5′-dcbpy)Cl) into the UiO-67 backbone [124]. A well-characterised catalyst for CO_2 reduction, the insertion of $Re(CO)_3$(5,5′-dcbpy)Cl) into UiO-67 demonstrated that catalyst addition did not influence the pXRD pattern, an effect most likely attributable to the comparable ligand lengths of $Re(CO)_3$(5,5′-dcbpy)Cl) and bpdc. Following an evaluation of photocatalytic behaviour in

CO_2-saturated acetonitrile in the presence of triethyl amine as a sacrificial reducing agent, high efficiency in the photocatalytic reduction of CO_2, represented by a turnover number of 10.9 over 12 h for selective reduction of CO_2 to CO, was demonstrated by the resulting MOF. This elevated catalytic activity, which inhibits the bimolecular catalytic decomposition pathway, can be attributed to site segregation in the $Re(CO)_3$(5,5′-dcbpy)Cl) catalyst. The incorporation of Fe_2(dcbdt)$(CO)_6$ into the UiO-66 framework by way of a post-synthetic exchange process was recently described by Ott et al. [125]. This process was evaluated by Energy-dispersive X-ray spectroscopy (EDX) and found to exhibit 14% incorporation, with the emergent MOF significantly more efficient compared to the analogous ligand for photochemical reduction using ascorbic acid which represents the sacrificial electron donor. The stabilisation of catalyst within the framework was used to explain the elevated activity levels observed.

5. Photocatalytic applications of MOFs

Over the past 10 years, MOFs have been successfully established as a new, promising class of heterogeneous photocatalytic materials. The use of MOFs in the photocatalytically driven degradation of organic pollutants and NO_x, antibacterial activity and generation of solar fuels and photoelectrochemical (PEC) energy highlights the impressive potential these materials possess [126–128]. Furthermore, there are several reported MOFs that have also been employed in the photocatalytic production of high-value chemicals under mild conditions. In these reports, the feasibility of fine tuning the MOF's energy band structure and surface functional group was proven. It is interesting to note that, although MOFs now stand on their own as a unique class of photocatalytic materials, they have been shown to be used as sacrificial precursors in the precisely controlled fabrication (phase, shape, morphology and porosity) of traditional semiconductor photocatalysts with greatly enhanced photocatalytic activity.

There are several excellent reviews that address the advances of MOFs in photodegradation of organic pollutants in wastewater [126, 129], water splitting [126, 128] and photoreduction of CO_2 [126, 128], where these materials' stability and light absorption properties are critically discussed. However, these reviews are limited in terms of delineating the design principle/criteria and the photocatalytic working mechanism, both of which are central to the development of new MOF photocatalysts having desirable properties for realisation in future practical applications. Accordingly, this section seeks to (1) present the primary processes involved in general photocatalytic reactions as they relate to the specific electronic band structures of MOFs, and (2) exemplify the photocatalytic applications of MOFs that were designed to address these fundamental photocatalytic processes.

5.1. Fundamental processes of photocatalysis as related to MOFs

Similar to classic photocatalysis theory developed for traditional semiconductor photocatalytic materials (**Figure 5**), MOF-based photocatalysis involves four fundamental processes of operation with additional distinct characteristics that can be intrinsically derived from their

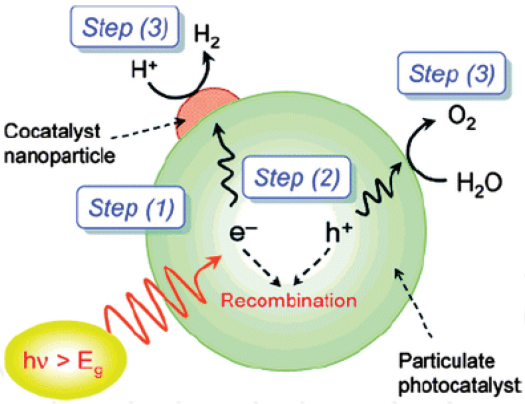

Figure 5. The major processes in classic photocatalysis system [136].

crystalline structure. These fundamental processes of operation, as they relate to MOF-based photocatalysis, are

1. Photoexcitation: In MOF-based photocatalysts, light absorption may occur either through the inorganic SBU or through the organic linker. MOFs typically have few absorption bands (broad bands are often seen) in the UV-Vis region depending on the chemical nature of the chromophore centres that arise from the inorganic SBUs or organic linkers. These absorption bands can often be ascribed to distinct π-π* transitions of the aromatic units in the organic linker or to metal-to-ligand (MLCT) or ligand-to-metal (LMCT) charge transfer transitions. Therefore, the band theory of semiconductors is not effective in describing the light absorption and subsequent transitions observed in MOF materials. On the other hand, it is more suitable to use molecular orbital theory, in which the peak of occupied molecular orbitals (HOMO) and the lowest unoccupied molecule orbital (LUMO) determine the so-called 'band gaps' of MOF photocatalysts [130]. As a result of the inorganic SBUs and organic linkers possessing distinct molecular orbitals, MOF photocatalysts often exhibit several discrete absorbance bands and the band with the lowest energy (longest wavelength) is used to define the band gaps. It is noted that LMCT effects are especially important for those MOFs that contain chromophore units originating at the organic linkers. Aside from determining the band gap energy, the energy positions of the HOMO and LUMO orbitals are critical for understanding the pathways and reaction products in photocatalytic reactions involving MOFs. This is critical as the photo-generated holes and electrons possess the same energetic levels as the HOMO and LUMO orbitals of MOFs, respectively.

2. Charge separation, transfer and transport processes: These processes, initiated and sustained through the absorption of excessive light energy, lead to positively and negatively charged excitons being separated and then transferred from the bulk to the surface of the photocatalyst. The efficiency of these processes decidedly relies on the type

of material, the material's crystallinity, as well as its particle size. For instance, high charge mobility is commonly associated with highly crystalline semiconductor materials, in which oriented charge mobility is observed. Structural deficiency in inorganic photocatalysts lies in the presence of chromophore centres, which may also serve as recombination centres where charge carriers are trapped and quenched leading to significant energy loss through realised heat. Semiconductor nanocrystals with small particle sizes generally possess satisfactory charge transfer performance; however, if particles are too small, then recombination may occur due to improved surface defects.

3. Surface reaction: Photo-generated charge carriers travel to the surface of the photocatalyst, in which they can be induced to participate in certain related chemical reactions or be collected by photoelectrodes in order to be passed to an external circuit. It is noted that the surface chemical reaction rate also influences the charge transition and transfer.

   The first step in a typical photocatalytic reaction is surface adsorption followed by the photocatalytic redox of the adsorbents. Taking into consideration the structural uniqueness of MOFs (functionalisable), remarkable surface properties by MOF photocatalyts are expected and, in fact, have been demonstrated [131–133]. Indeed, Natarajan, et al. investigated the adsorption and the catalytical photodegradation behaviour of different dyes on three Cd-containing MOFs, namely $Cd_2(4,4'\text{-bpy})_3(S_2O_3)_2$, $Cd_2(4,4'\text{-bpy})_{2.5}(S_2O_3)_2$ and $[Cd(4,4'\text{-bpy})(H_2O)_2(S_2O_3)]\cdot 2H_2O$ [134]. In this report, the anionic (orange G, methyl orange) and cationic dyes (methylene blue, methyl violet and brilliant blue R) exhibited distinct surface adsorption capacity and photocatalytic activity. By analyzing the adsorption data using the Langmuir adsorption model, the authors reported that the anionic dyes (e.g., sulphonated) were significantly more adsorbed by $Cd_2(4,4'\text{-bpy})_3(S_2O_3)_2$, $Cd_2(4,4'\text{-bpy})_{2.5}(S_2O_3)_2$ and $[Cd(4,4'\text{-bpy})(H_2O)_2(S_2O_3)]\cdot 2H_2O$ in the dark with no apparent adsorption occurring for the non-cationic dyes. Furthermore, it was determined that the dye molecule adsorption did not lead to any structural changes in the cadmium thiosulfphte MOF materials, but rather weak electronic interactions were observed. The hydroxyl radicals play crucial roles in breaking down the anthraquinonic anionic dyes while surface-controlled N-de-ethylation reaction mechanism was proposed to explain the stepwise decomposition of cationic dyes through serials intermediates, where MLCT arisen from HOMO of filled d^{10} orbitals of Cd and ligand-associated LUMO plays dominant roles. [135].

4. Charge carrier recombination: Charge carrier recombination is a process in which photogenerated electrons and holes will recombine and, as a result, release energy that was gained during excitation in the form of fluorescence or heat. The energy emitted during recombination can be captured and interpreted using photoluminescence (PL) spectroscopy. The recombination of charge carriers accounts for the largest energy loss in most photocatalytic and PEC systems and remains as one of the greatest challenges necessary to tackle. In general, the recombination of charge carriers occurs in both the bulk and surface of the photocatalyst; therefore, it is very important to study the bulk and surface recombination when sorting recombination. The recombination can be largely suppressed by decreasing the photocatalyst particle size or by applying an external energy bias. These

methods have proven effective for both classical semiconductors as well as in MOF photocatalysts. It is noted that surface metallisation using noble metals has also been reported useful [131, 136–138].

5.2. Extensive application of MOFs in photocatalysis

5.2.1. Photocatalytic decomposition of organic pollutants

The semiconducting behaviour was first proposed and observed on MOF-5 which displayed comparable specific activity (phenol decomposition per metal atom) to TiO_2-P25 and ZnO in photodegration of phenol under UV illumination (125 W medium pressure Hg lamp) but the apparent mass photoactivity was weaker than TiO_2 and ZnO [139]. The photocatalytic phenol decomposition was proposed to follow the LMCT mechanism, in which photoexcited holes oxidise phenol to form phenol cation or phenol is oxidised by active oxygen species generated from photo-generated CB electrons inject to dissolved oxygen. Encouraged by the promising photocatalysis on MOF-5, a variety of UV-responsive MOFs have been developed and examined for photocatalytic decomposition of organic pollutants in water [129]. In these semiconducting MOFs, d-block and f-block metals, including Mn, Fe, Co, Ni, Zn, Cd, Ti, Zr and Gd, are frequently applied, while the organic linkers are found determining their bandgap and photocatalytic activity due to the LMCT mechanism. Another important factor influencing the photocatalytic activity is the selective adsorption of organic pollutant compounds owing to the static electrical interaction or shape selectivity.

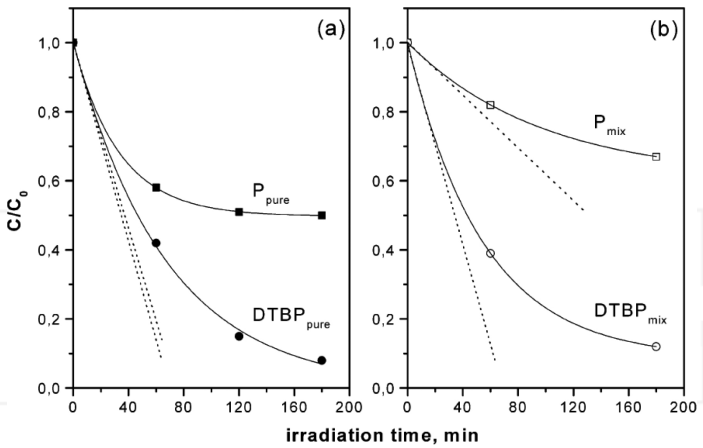

Figure 6. UV-driven photodegradation curves of phenol (P) and 2,6-di-*tert*-butylphenol (DTBP), obtained using MOF-5 as a photocatalyst. (a) Curves correspond to photodegradation of 40 mg L^{-1} of the pure species, (b) curves correspond to competitive photodegradation (irradiation of a mixture of 20 mg L^{-1} of both molecules). Solid lines are the best fit to the experimental data obtained with a first-order exponential decay. Dotted straight lines show the initial degradation rates [136].

The microporous MOF-5 showed (**Figure 6**) an interesting reverse shape selectivity in photocatalytic decomposition of mixed solution of 2,6-di-*tert*-butylphenol (DTBP) and phenol(P). Under UV irradiation, the large DTBP molecule underwent faster photodegradation than small phenol molecule in the mixed solution, which was attributed to the phenol diffusing into the interior channels of MOF-5 and less exposure to light than DTBP which cannot diffuse into the MOF-5's micropores [140].

The adsorption and photocatalytical degradation of different types of dyes on the MOFs containing similar Cd cluster vary along with the organic linkers. It was found the sulphonated anionic dyes were significantly adsorbed by $Cd_2(4,4'\text{-bpy})_3(S_2O_3)_2$, $Cd_2(4,4'\text{-bpy})_{2.5}(S_2O_3)_2$ and $[Cd(4,4'\text{-bpy})(H_2O)_2(S_2O_3)]\cdot 2H_2O$ in the dark, but the photodegradation performance was not examined. Despite these MOFs almost did not adsorb non-sulphonated cationic dyes (e.g., methylene blue, MB) [134], they showed comparable activity to TiO_2 in the UV-driven photodegradation of non-sulphate dyes because of the complex photocatalysis mechanism involving active oxygen species arisen from bandgap excitation and dye photosensitisation. The same mechanism was also proposed in the X3B photodegradation on $[Mn_3(btc)_2(bimb)_2]\cdot 4H_2O$ and $[Co_3(btc)_2(bimb)_2]\cdot 4H_2O$ [141], and rhodamine B photodegradation on $[Ag(bipy)(UO_2)(bdc)_{1.5}]$ (bipy=2,2′-bipyridyl, bdc=1,4-benzenedicarboxylate) and $[Ag_2(phen)_2UO_2(btec)]$ (phen=1,10-phenanthroline, btec=1,2,4,5-benzenetetracarboxylate)[17]. It is worth noting the$[Co_3(btc)_2(bimb)_2]\cdot 4H_2O$ exhibited better photoactivity than the $[Mn_3(btc)_2(bimb)_2]\cdot 4H_2O$ despite the Co-based MOF (~4.04 eV) possessed larger bandgap than the Mn-based MOF (~3.72 eV). The reverse activity order to the bandgap is because Co-based MOF possesses two additional d-d spin-allowed LMCT transition of Co^{2+} within 400–800 nm band region, besides the aforementioned complex mechanism (dye-sensitising and active oxygen species, **Figure 7**) [142].

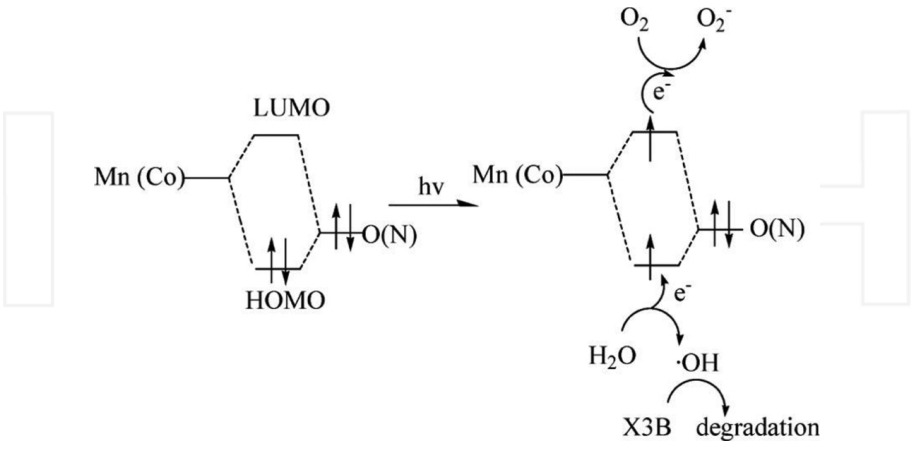

Figure 7. A simplified model of photocatalytic reaction mechanism of $[Mn_3(btc)_2(bimb)_2]\cdot 4H_2O$ and $[Co_3(btc)_2(bimb)_2]\cdot 4H_2O$ [143].

In order to maximise the visible-light harvesting in solar spectrum, intensive efforts have been made to develop visible-light-responsive MOFs via various strategies, such as modifying metal nodes, functionalising organic linkers, using hybrid linkers as well as constructing composite photocatalysts [143]. Although the light absorption of MOF-5 may be extended to 400 nm, its visible-light-driven photocatalysis is negligible due to the large bandgap (~3.4 eV) but its bandgap may be reduced largely once the bdc linker is functionalised [144, 145]. Diverse visible-light-responsive and stable MOFs have recently been tested in photocatalytic reactions, particularly in dye decomposition.

The present investigated visible-light-responsive MOFs may be roughly categorised as follows [126–129, 146, 147]:

1. Simple MOFs, sMIL-88A, MIL (TM) (TM=Fe, Cr), NTU-9, Fe_2(bhbdh),
2. MOFs with hybrid organic linkers: $[Zn_4(O)(tdc)_3(4,4'\text{-bimb})_4]\cdot 5.25H_2O\cdot CH_3OH$, Cu^{II}(salimcy)]($Cu^{I}I)_2\cdot$DMF, Cu(Br-ip)(bitmb)(H_2O), etc.
3. Linker-functionalised. Amino-group functionalised NH_2-MIL-125[Ti] and MOF-5, etc.
4. Node-substituted MOFs. For example, X_4Y–MOF-5 (X = Zn, Cd, Be, Mg, Ca, Sr, Ba; Y = O, S, Se, Te), etc.
5. Metal-substituted or ion exchanged zeolitic MOFs. Cu/ZIF-67.
6. Heterojunctions. For instance, Fe_3O_4@MIL-100(Fe), Bi_2WO_6/UiO-66, C_3N_4/MOF-5, Fe3O4@HKUST-1, UiO-66/CdS [148], Ag_2O/MOF, etc.
7. Polyoxometalate-based MOFs, for example $[Cu_8(1,3\text{-btp})_8[Mo_{12}O_{46}(AsPh)_4]_2]\cdot 3H_2O$, $[CoCl_{0.5}(H_2O)_{0.5}(Hdppzc)_2](PW_{12}O_{40})_{0.5}\cdot 3.5H_2O$, $[Cu(II)_2Cu(I)_3(OH)_4(H_2O)_2(tpt)_4](PW_{12}O_{40})$, etc.
8. Photosensitised MOFs. Photosensitisation is widely observed in various MOFs once dye is involved in the photocatalytic reaction. It is interesting that the photosensitisation effect may coexist within a complex MOF, such as CuPW and CuPM.
9. Surface metalised MOFs. The plasmonic effect of the nanosized metal particle sit on the MOF surface may endow visible light response to the host MOF. For example, Au@UiO-66(NH_2)[10] and Ag/AgCl@ZIF-8 [149].

5.2.2. Photocatalytic selective redox in organic synthesis

Normally, photocatalytic oxidation is a non-selective reaction on conventional inorganic photocatalyst because the photo-generated redox radical is non-selective. However, due to the tuneable HUMO and LUMO energy levels, LMCT effect, shape-selective adsorption and orientation of organic linkers, given proper design of structure and components of the MOF photocatalysts, they may enable selective oxidation of organic substrates under ambient conditions. Under UV irradiation and existence of a unique porous MOF having 3D structure, obtained from tin(IV)–porphyrin struts connected to Zn atoms and formats linking Sn^{IV} centres [150], 1,5-dihydroxynaphthalene can be oxidised into 5-hydroxynaphthalene-1,4-

dione, while different organic sulphides into organic sulphoxides rather than sulphones, respectively. In the both cases, the yield and selectivity are nearly 100%. In this MOF photocatalyst, the anchored tin(IV)-porphyrin serves as photoactive site and the tin(IV)-porphyrin itself is a proven photocatalyst for such reactions yet suffers from fast deactivation. However, the heterogeneous MOF showed remarkably higher product yield, selectivity and stability than the tin(IV)–porphyrin in homogeneous system.

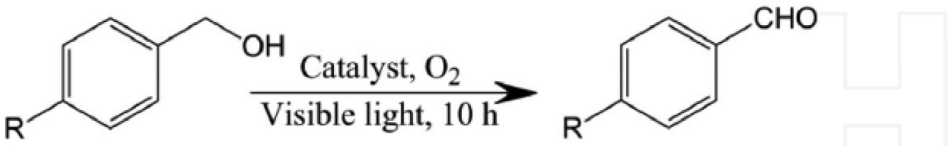

Entry	–R	Conversion (%)		Selectivity (%)
		NH_2-MIL-125(Ti)	Ni-doped NH_2-MIL-125(Ti)	
1	$–NO_2$	8.2	10.5	>99
2	–Cl	11.8	20.6	>99
3	–H	12.5	21.5	>99
4	$–CH_3$	25.8	43.2	>99
5	$–OCH_3$	42.5	47.4	>99

[a]Reaction conditions: 50 mg of catalyst and 0.3 mmol of aromatic alcohol in 6 ml of BTF at room temperature for 10 h.

Table 1. Aerobic photocatalytic oxidation of aromatic alcohols over NH_2-MIL-125(Ti) and Ni-doped NH_2-MIL-125(Ti) upon visible light irradiation[a] [152].

Upon visible light irradiation, the oxidation of aerobic amines was obtained using NH_2-MIL-125(Ti) as active photocatalysts and the photocatalyst was evidenced as stable catalyst in such photocatalytic reaction [132]. Photo-generated Ti^{3+} and $.O^{2-}$ are supposed to be involved in the reaction of amines transformation through a five-step redox mechanism. As shown in the schematic mechanism (**Figure 8**), there are five steps for the photocatalytic oxidation of amines using NH_2-MIL-125(Ti) as photocatalyst. The first step shows the transformation of electron to Ti-O oxo-cluster to create Ti^{3+} moiety. This step occurs upon the irradiation of the aminoterephthalic acid (ATA) ligand. In the second step, the obtained Ti^{3+} would react with O_2 to create $\cdot O_2^-$ while Ti^{3+} was oxidised back to Ti^{4+}. It should be noted that amines in the third step will able to provide electron followed by a deprotonation process to form the carbon-centered radical. In the fourth step, the aldehyde will be obtained by the interaction between the photo-generated carbon cantered radical and the $.O_2^-$. Finally (step 5), the nucleophilic attack on aldehydes through the unreacted amines will therefore yield the corresponding imines via dehydration step. Some other by-product such benzaldoximeis can

be observed which occurs due to the reaction between carbon-centred radical and O_2 which then followed by a dehydration step [132].

Similarly, the NH_2-MIL-125(Ti) and Ni-doped NH_2-MIL-125(Ti) photocatalysts can also transform aromatic alcohols to their corresponding aldehydes with almost absolute selectivity using O_2 as the oxidant under visible light irradiation [151]. As shown in **Table 1**, Compared with the parent catalyst NH_2-MIL-125(Ti), Ni-doped NH_2-MIL-125(Ti) significantly enhances the photocatalytic activity for the selective oxidation of aromatic alcohols. The photoelectrochemical characterisation results suggest that the doping of Ni nanoparticles into NH_2-MIL-125(Ti) can improve the visible-light harvesting, charge separation and electron transport of the resultant catalyst, which lead to the enhanced photocatalytic activity.

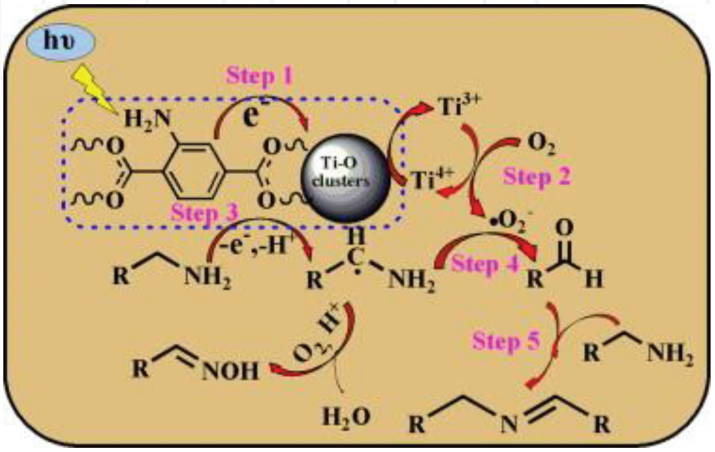

Figure 8. Suggested photocatalytic mechanism of the amines oxidation using NH_2-MIL-125(Ti).

5.2.3. Photoelectrochemical application

It has recently evidenced that MOFs may be promising materials in photoelectrochemical catalysis or photoelectrochemical cells for enhanced solar energy conversion. The intrinsic properties of the MOFs, peculiarly the linkers, would endow interesting properties to the pure or hybridised MOFs.

As shown in **Figure 9(a)**, a metal oxide semiconductor supported on MOF core/shell heterostructure (e.g., ZnO@ZIF-8 nanorod) was ever effectively synthesised via a simple self-template method [151]. In such producer, ZnO nanorods do not act only as template but they provide Zn^{2+} ions in order to obtain ZIF-8 [150]. In such method, the reaction temperature and the solvent compaction were found to play a significant role in order make ZnO@ZIF-8 heterostructures. It has observed that such obtained materials show a diverse photoelectrochemical response stewards these hole scavengers to hole scavengers. The reason behind such phenomena is the limitation of the aperture of the ZIF-8 shell, as shown **Figure 9(b)**, which is

different from ZnO nanorod arrays. Such interesting properties enable the composite electrode to be successfully used for the H_2O_2 detection, as shown in **Figure 9(c)**.

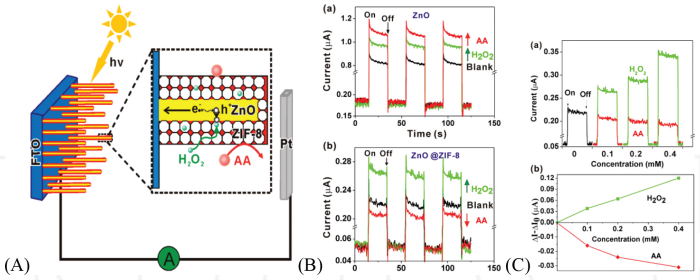

Figure 9. (a) schematic configuration of an photoelectrodes of ZnO@ZIF-8 nanorod array; (b) Photocurrent response of ZnO nanorod and ZnO@ZIF-8 nanorod arrays against H_2O_2 (0.1 mM) and AA (0.1 mM); (c) Photocurrent responses of the ZnO@ZIF-8 nanorod array in the presence of H_2O_2 and AA with different concentrations. (b) ΔI − ΔI0 curves in the presence of H_2O_2 and AA with the concentrations as function.

Lee et al. fabricated Cu-based copper(II) benzene-1,3,5-tricarboxylate layer using a layer-by-layer (LBL) method, and applied as a light-absorbing layer in TiO_2-based solar cells [152]. The TiO_2-based solar cell fabricated was the first report using iodine-doped Cu-MOFs which act as active layer. The reported confirmed that the cell performance with J_{sc} = 1.25 mA cm^{-2} and Eff = 0.26% using illumination of 1 sun radiation was obtained. On the other hand, the cell contains undoped MOF layer showed J_{sc} = 0.05 mA cm^{-2} and Eff = 0.008%. The results showed that the iodine doping considerably reduces the charge-transfer resistance through the

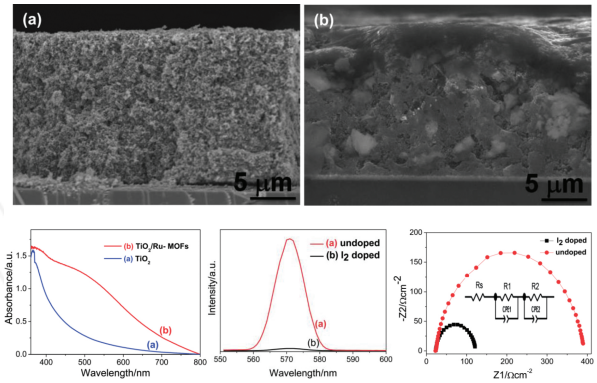

Figure 10. SEM cross-sectional views of doctor blade TiO_2 film using FTO glass (a) before and (b) after, deposition of Ru-MOFs for 10 LbL cycles; UV-visible spectrum of doctor blade TiO_2 film on FTO glass (a) before and (b) after, deposition of Ru-MOFs for 10 LbL cycles; emission spectrum of TiO_2/Ru-MOFs film (a) before and (b) after, doping MOFs with iodine. Excitation at wavelength ~535 nm. Nyquist plots of Ru-MOF-sensitized cell under open circuit and 1 sun illumination conditions. Iodine doping of MOFs is showing the facilitation of charge transfer process. Dots are experimental data and the solid lines are the fitted curves using an equivalent circuit shown in set [155].

TiO_2/MOF/electrolyte interface, as confirmed by electrochemical impedance spectroscopy. The similar LBL was also applied by the same group to fabricate Ru-based MOFs photoelectrode for solar cell application [153]. They observed the similar phenomena as the Cu-MOF solar cell, confirming the I-doped Ru-MOF possesses enhanced light absorption, reduced charge recombination and higher charge conductivity which contribute to enhanced solar energy efficiency (**Figure 10**).

5.2.4. Photocatalytic oxidation of nitric oxide (NO) and antibacterial activity

It was reported that one-pot microwave synthesised Ag@NH_2-MOP(Ti) exhibited excellent activity in visible-light-driven photocatalytic NO oxidisation, much higher than NH_2-MOP(Ti) and twofold than on *N*-doped TiO_2, as shown in **Figure 11(a)**. The NH_2-MOP(Ti) absorbed visible lights to generate photoelectrons and holes, accompanied by producing HO• and O_2^- active species for the subsequent NO oxidation into NO_3^-. The supported Ag nanoparticles allowed assembly of NH_2-MOP(Ti) polymer, favoured light absorbance via multiple reflections and facilitated photoelectrons transfer with inhibited recombination of photo-generated charge transporters, which lead to enhance the photocatalytic activity for NO oxidation. Besides the high activity, the Ag@NH_2-MOP(Ti) also showed strong durability and could be used repetitively without significant decrease in activity (**Figure 11(b)**). No obvious changes on the physicochemical properties and morphology of the samples after the cycled reaction were observed. The slight decrease of activity could be mainly attributed to the adsorption of HNO_3 product onto the photocatalyst. The Ag@NH_2-MOP(Ti) was claimed to be able to photocatalytically inactivate bacteria, whereas it remains unclear if the bactericidal effects were induced by Ag or the MOF because Ag has intrinsic antibacterial function and the photocatalytically antibacterial activity was not examined. The research verifies the feasibility to apply pristine and composite MOFs for photocatalytic removal of gaseous pollutants which has not been well explored.

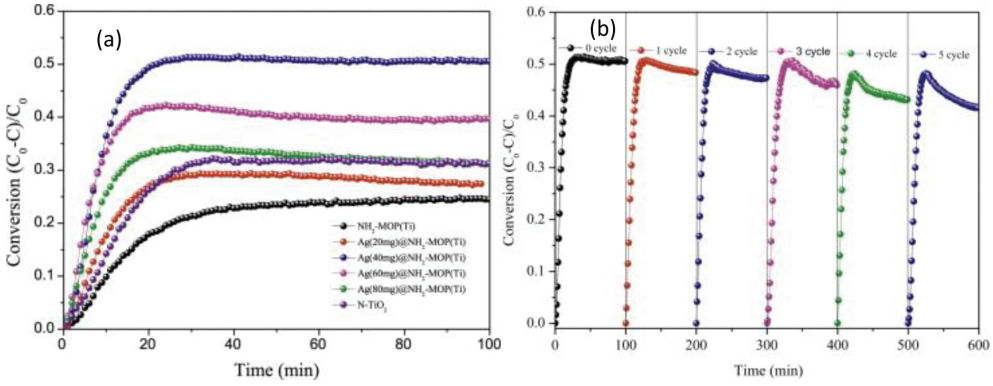

Figure 11. (a) Photocatalytic NO oxidation profiles on N-TiO_2, NH_2-MOP(Ti) and Ag@NH_2-MOP(Ti); (b) recycling photocatalytic NO oxidation tests on Ag@NH_2-MOP(Ti) under visible light ($\lambda \geq 420$ nm).

http://dx.doi.org/10.5772/63489

5.2.5. Photocatalytic reduction of metal cations for metal recovery or detoxcity

Shi et al. confirmed that due to the direct excitation of Fe_3-μ_3-oxo clusters in the MIL-88B (Fe) MOFs, this material is a good candidate for the photocatalytic reduction of Cr(VI) using visible light irradiation [154]. It is clear that the amine-functionalised MIL-88B (Fe) MOFs display a better photocatalytic efficiency for the reduction of Cr(VI) under visible-light irradiation compared to MIL-88B (Fe). As proposed in **Figure 12**, the direct excitation of Fe_3-μ_3-oxo clusters lead to excite the amine functionality in NH_2-MIL-88B (Fe). In such phenomena, the electron will be then transferred to Fe_3-μ_3-oxo clusters, which is considered to be responsible for the enhancement of the reduction of Cr(VI) photocatalytically.

With proper design, a stable and active MOF as photocatalyst can be prepared. For example, Shen et al. synthesised Pd@UiO-66(NH_2) nanocomposite, on which highly dispersed Pd nanoparticles having a diameter size between 3 and 6 nm were immobilised into UiO-66(NH_2) using hydrothermal preparation method. Obtained Pd nanoparticles supported on UiO66 show an excellent photocatalytic activity for the reduction of Cr(VI) compared to unsupported Pd nanoparticles. The reason of such good activities can be attributed to the fact that the Pd nanoparticles were well dispersed in the surface of UiO66-NH_2, which leads to improve the light harvesting and better efficient separation of the photo-generated electron-hole pairs [155]. Furthermore, Pd nanoparticles supported on UiO66-NH_2 could also be applied to photodegrade other types of organic pollutants such methylene blue (MB) and methyl orange (MO) with enhanced activity in the binary system. The synergetic effect between photocatalytic oxidation and reduction can be individually consumed photo-generated holes and electrons [156].

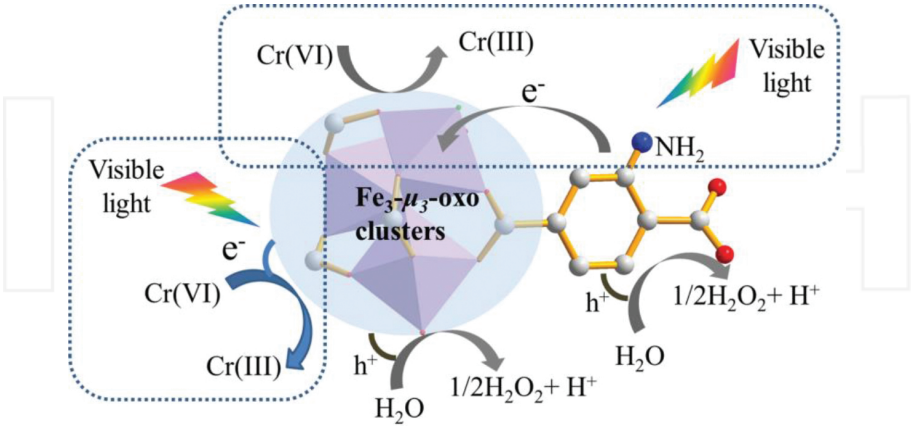

Figure 12. Suggestion dual excitation ways mechanism for photocatalytic reduction of Cr(VI) on NH_2–MIL-88B (Fe) [154].

6. Perspectives

As emerging photocatalytic materials, semiconducting MOFs exhibited promising future and have attracted extensive research interest, whereas they face significant challenges for widespread application. In order to tackle these issues, great research efforts are necessary to put on:

1. Design the energy bandgap and band positions through tuning the metal or metal cluster nodes as well as target-directed design of the ligands.
2. The incorporation of inorganic semiconductors, polymer semiconductors and surface metallisation may enrich the family of the MOFs photocatalysts with desirable performance because of their ability in fine tuning the energy alignment of the materials as well as the charge carrier transportation.
3. Extend the photocatalytic application fields of MOF-based photocatalysts. Recovery of noble metals from metallurgy industries and heavy metal cations from wastewater or soil, the bactericidal applications and photocatalytic cleanup of indoor air are highly demanding and can be strong spur for the extended applications of MOFs. Artificial photosynthesis, including water splitting and photoreduction of CO_2, represents an emerging and ever-fast increasing application of MOFs. The direct capture and photoreduction of CO_2 from air might be realisable in terms of the selective adsorption and the separated redox active sites of the MOFs, which enable the designed MOFs to mimic natural plants, for conducting light oxidation reaction on the external surface or shallow pores of MOFs yet reductive 'dark' reaction within the MOFs' channels. The photocatalytic selective redox in production of value-added advanced chemicals or pharmaceutical intermediates would open new and sustainable pace for MOFs' applications.
4. Develop MOF-based photocatalysis devices, for example, MOF solar cells and photocatalytic-based sensors, where photoelectrochemical signals may be used to diagnose the specific chemical substrates.
5. Develop and apply spectral and photoelectrochemical characterisation techniques, in particular transient characterisations, for precisely exploring the exact photocatalytic and photoelectrochemical catalysis mechanism.
6. Demonstrate the potentials of MOF-based photocatalysts at pilot scale. There are a large number of evidences to confirm the potentials of the photocatalytic applications of MOFs at laboratory-scale tests while the large-scale applications still are not convinced due to the high cost of MOFs and the suspicious stability of such complex inorganic-organic networks. The involvement of industrial partners and diverse stakeholders would be more persuasive to commercialise MOFs in the utilisation of planet-saving solar energy photocatalysis technologies.

The ever-increasing expansion and enormous progress of MOFs have been observed since the discovery of first MOFs. It is undoubted the MOFs would be an important class of alternative photocatalysts relative to the conventional inorganic semiconductor photoca-

talysts, despite that various strategies still are under development and are verifying to tackle the present challenges associated with MOFs.

Author details

Ahmad Alshammari[1*], Zheng Jiang[2*] and Kyle E. Cordova[3]

*Address all correspondence to: aalshammari@kacst.edu.sa and z.jiang@soton.ac.uk

1 Materials Science Research Institute (MSRI), King Abdulaziz City for Science and Technology (KACST), Riyadh, Saudi Arabia

2 Faculty of Engineering and the Environment, University of Southampton, Southampton, UK

3 Department of Chemistry, University of California-Berkeley, Berkeley, California, USA

References

[1] Ma S, Zhou H-C. Gas storage in porous metal–organic frameworks for clean energy applications. Chem. Commun. 2010; 46:44–53. DOI: 10.1039/B916295J.

[2] Li J-R, Sculley J, Zhou H-C. Metal-organic frameworks and porous polymer networks for carbon capture. Chem. Rev. 2012; 112:869–932.

[3] Makal TA, Li J-R, Lu W, Zhou H-C. Fine-tuning the balance between crystallization and gelation and enhancement of CO2 uptake on functionalized calcium based MOFs and metallogels. Chem. Soc. Rev. 2012; 41:7761–7779.

[4] Liu C, Li F, Ma L-P, Cheng H-M. Advanced materials for energy storage. Adv. Mater. 2010; 22:E28–E62.

[5] Li J-R, Kuppler RJ, Zhou H-C. Selective gas adsorption and separation in metal-organic frameworks. Chem. Soc. Rev. 2009; 38:1477–1504.

[6] Zacher D, Shekhah O, Woll C, Fischer RA. Thin films of metal-organic frameworks. Chem. Soc. Rev. 2009; 38:1418–1429.

[7] Bradshaw D, Garai A, Huo J. Metal–organic framework growth at functional interfaces: thin films and composites for diverse applications. Chem. Soc. Rev. 2012; 41:2344–2381.

[8] Cui Y, Yue Y, Qian G, Chen B. Confinement of pyridinium hemicyanine dye within an anionic metal-organic framework for two-photon-pumped lasing. Chem. Rev. 2012; 112:1126–1162.

[9] Chen L, Tan K, Lan Y-Q, Li S-L, Shao K-Z, Su ZM. Self-assembly versus stepwise synthesis: heterometal-organic frameworks based on metalloligands with tunable luminescence properties. Chem. Commun. 2012; 48:5919–5921.

[10] Lee JY, Farha OK, Roberts J, Scheidt KA, Nguyen ST, Hupp JT. Metal-organic framework materials as catalysts. Chem. Soc. Rev. 2009; 38:1450–1459.

[11] Ma L, Abney C, Lin W. Enantioselective catalysis with homochiral metal-organic frameworks. Chem. Soc. Rev. 2009; 38:1248–1256.

[12] O'Keeffe M, Yaghi OM. Deconstructing the crystal structures of metal-organic frameworks and related materials into their underlying nets. Chem. Rev. 2012; 112:675–702. DOI: dx.doi.org/10.1021/cr200205j

[13] Shibata YJ. Coll. Sci., Imp. Univ. Tokyo. 1916; 37:1–31.

[14] Keggin JF, Miles FD. Structures and formulae of the Prussian blues and related compounds. Nature. 1936; 137:577–578. DOI:10.1038/137577a0

[15] Ferey G. Microporous solids: from organically templated inorganic skeletons to hybrid frameworks…ecumenism in chemistry. Chem. Mater. 2001; 13:3084–3098.

[16] Janiak C. Engineering coordination polymers towards applications. Dalton Trans. 2003; 2781–2804. DOI:10.1039/B305705B

[17] Hofmann KA, Kuspert FA. Z. Compounds of hydrocarbons with metal salts. Anorg. Allg. Chem. 1897; 15:204–207. DOI:10.1002/zaac.18970150118

[18] Powell HM, Rayner JH. Clathrate compound formed by benzene with an ammonia–nickel cyanide complex. Nature. 1949; 163:566–567. DOI:10.1038/163566a0

[19] Iwamoto T, Miyoshi T, Miyamoto T, Sasaki Y, Fujiwara S. The metal ammine cyanide aromatics clathrates. I. The preparation and stoichiometry of the diamminemetal(II) tetracyano-niccolate(II) dibenzene and dianiline. Bull. Chem. Soc. Jpn. 1967; 40:1174–1178. DOI:10.1246/bcsj.40.1174

[20] Kinoshita Y, Matsubara I, Higuchi T, Saito Y. The crystal structure of Bis(adiponitrile)copper(I) Nitrate. Bull. Chem. Soc. Jpn. 1959; 32:1221–1226. DOI: http://doi.org/10.1246/bcsj.32.1221

[21] Yaghi OM, Li GM, Li HL. Selective binding and removal of guests in a microporous metal–organic framework. Nature. 1995; 378:703–706. DOI:10.1038/378703a0

[22] Li H, Eddaoudi M, O'Keeffe M, Yaghi OM. Design and synthesis of an exceptionally stable and highly porous metal-organic framework. Nature. 1999; 402:276–279. DOI: 10.1038/46248

[23] Kaye SS, Dailly A, Yaghi OM, Long JR. Impact of preparation and handling on the hydrogen storage properties of Zn4O(1,4-benzenedicarboxylate)3 (MOF-5). J. Am. Chem. Soc. 2007; 129:14176–14177. DOI:10.1021/ja076877g

[24] Chae HK, Siberio-Perez DY, Kim J, Go Y, Eddaoudi M, Matzger AJ, O'Keeffe M, Yaghi OM. A route to high surface area, porosity and inclusion of large molecules in crystals. Nature. 2004; 427:523–527. DOI:10.1038/nature02311

[25] Furukawa H, Ko N, Go YB, Aratani N, Choi SB, Choi E, Yazaydin AO, Snurr RQ, O'Keeffe M, Kim J, Yaghi OM. Ultrahigh porosity in metal-organic frameworks. Science. 2010; 329:424–428. DOI:10.1126/science.1192160

[26] Chen BL, Liang CD, Yang J, Contreras DS, Clancy YL, Lobkovsky EB, Yaghi OM, Dai S. A microporous metal-organic framework for gas-chromatography separation of alkane. Angew. Chem. Int. Ed. 2006; 45:1390–1393. DOI:10.1002/anie.200502844

[27] Lee JY, Pan L, Huang XY, Emge TJ, Li J. A systematic approach to building highly porous, noninterpenetrating metal–organic frameworks with a large capacity for adsorbing H2 and CH4. Adv. Funct. Mater. 2011; 21:993–998. DOI:10.1002/adfm.201001790

[28] Wang XF, Wang Y, Zhang YB, Xue W, Zhang JP, Chen XM. Layer-by-layer evolution and a hysteretic single-crystal to single-crystal transformation cycle of a flexible pillared-layer open framework. Chem. Commun. 2012; 48:133–135. DOI:10.1039/C1CC15891K 29. Koh K, Wong-Foy AG, Matzger AJ. A porous coordination copolymer with over 5000 m2/g BET surface area. J. Am. Chem. Soc. 2009; 131:4184–4185. DOI:10.1021/ja809985t

[29] Ferey G, Mellot-Draznieks C, Serre C, Millange F, Dutour J, Surble S, Margiolaki I. A chromium terephthalate-based solid with unusually large pore volumes and surface area. Science. 2005; 309:2040–2042. DOI:10.1126/science.1116275

[30] Hong DY, Hwang YK, Serre C, Ferey G, Chang JS. Porous chromium terephthalate MIL-101 with coordinatively unsaturated sites: surface functionalization, encapsulation, sorption and catalysis. Adv. Funct. Mater. 2009; 19:1537–1552. DOI:10.1002/adfm.200801130

[31] Zhao D, Yuan DQ, Sun DF, Zhou HC. Stabilization of metal-organic frameworks with high surface areas by the incorporation of meso cavities with micro windows. J. Am. Chem. Soc. 2009; 131:9186–9187. DOI:10.1021/ja901109t

[32] Chui SSY, Lo SMF, Charmant JPH, Orpen AG, Williams ID. A chemically functionalizable nanoporous material. Science. 1999; 283:1148–1150. DOI:10.1126/science.283.5405.1148

[33] Schlichte K, Kratzke T, Kaskel S. Improved synthesis, thermal stability and catalytic properties of the metal-organic framework compound Cu3(BTC)2. Micropor. Mesopor. Mater. 2004; 73:81–88. DOI:10.1016/j.micromeso.2003.12.027

[34] Alaerts L, Seguin E, Poelman H, Thibault-Starzyk F, Jacobs PA, De Vos DE. Probing the Lewis acidity and catalytic activity of the metal-organic framework [Cu-3(btc)(2)] (BTC = benzene-1,3,5-tricarboxylate) Chem. Eur. J. 2006; 12:7353–7363. DOI:1854/5954

[35] Kramer M, Ulrich SB, Kaskel S. Synthesis and properties of the metal-organic framework Mo3(BTC)2(TUDMOF-1). J. Mater. Chem. 2006; 16:2245–2248. DOI:10.1039/B601811D

[36] Xie LH, Liu SX, Gao CY, Cao RG, Cao JF, Sun CY, Su ZM. Mixed-valence Iron(II, III) trimesates with open frameworks modulated by solvents. Inorg. Chem. 2007; 46:7782–7788. DOI:10.1021/ic062273m

[37] Murray LJ, Dinca M, Yano J, Chavan S, Bordiga S, Brown CM, Long JR. Highly-selective and reversible O2 binding in Cr3(1,3,5-benzenetricarboxylate)2. J. Am. Chem. Soc. 2010; 132:7856–7857. DOI:10.1021/ja1027925

[38] Dietzel PDC, Morita Y, Blom R, Fjellvag H. An in situ high-temperature single-crystal investigation of a dehydrated metal–organic framework compound and field-induced magnetization of one-dimensional metal–oxygen chains. Angew. Chem. Int. Ed. 2005; 44:6354–6358. DOI:10.1002/anie.200501508

[39] Rowsell JLC, Yaghi OM. Effect of functionalization, catenation, and variation of the metal oxide and organic linking units on the low-pressure hydrogen adsorption properties of metal−organic frameworks. J. Am. Chem. Soc. 2006; 128:1304–1315. DOI: 10.1021/ja056639q

[40] Caskey SR, Wong-Foy AG, Matzger AJ. Dramatic tuning of carbon dioxide uptake via metal substitution in a coordination polymer with cylindrical pores. J. Am. Chem. Soc. 2008; 130:10870–10871. DOI:10.1021/ja8036096

[41] McKinlay AC, Xiao B, Wragg DS, Wheatley PS, Megson IL, Morris RE. Exceptional behavior over the whole adsorption−storage−delivery cycle for no in porous metal organic frameworks. J. Am. Chem. Soc. 2008; 130:10440–10444. DOI:10.1021/ja801997r

[42] Henschel A, Gedrich K, Kraehnert R, Kaskel S. Catalytic properties of MIL-101. Chem. Commun. 2008; 4192–4194. DOI:10.1039/B718371B

[43] Kim J, Bhattacharjee S, Jeong KE, Jeong SY, Ahn WS. Selective oxidation of tetralin over a chromium terephthalate metal organic framework, MIL-101. Chem. Commun. 2009; 3904–3906. DOI:10.1039/B902699A

[44] Kitaura R, Onoyama G, Sakamoto H, Matsuda R, Noro S, Kitagawa S. Immobilization of a metallo schiff base into a microporous coordination polymer. Angew. Chem. Int. Ed. 2004; 43:2684–2687. DOI:10.1002/anie.200352596

[45] Fletcher AJ, Thomas KM, Rosseinsky MJ. Flexibility in metal-organic framework materials: impact on sorption properties. J. Solid State Chem. 2005; 178:2491–2510. DOI:10.1016/j.jssc.2005.05.019

[46] Kitagawa S, Uemura K. Dynamic porous properties of coordination polymers inspired by hydrogen bonds. Chem. Soc. Rev. 2005; 34:109119. DOI:10.1039/B313997M

[47] Horike S, Shimomura S, Kitagawa S. Soft porous crystals. Nat. Chem. 2009; 1:695–704. DOI:10.1038/nchem.444

[48] Sing KSW, Everett DH, Haul RAW, Moscou L, Pierotti RA, Rouquerol J, Siemieniewska T. Reporting physiosorption data for gas/solid systems with special reference to determination of surface area and porosity. Pure Appl. Chem. 1985; 57:603–619. DOI:http://dx.doi.org/10.1351/pac198557040603.

[49] Li D, Kaneko K. Hydrogen bond-regulated microporous nature of copper complex-assembled microcrystals. Chem. Phys. Lett. 2001; 335:50–56. DOI:10.1016/S0009-2614(00)01419-6

[50] Kitaura R, Seki K, Akiyama G, Kitagawa S. Porous coordination-polymer crystals with gated channels specific for supercritical gases. Angew. Chem. Int. Ed. 2003; 42:428–431. DOI:10.1002/anie.200390130

[51] Horike S, Tanaka D, Nakagawa K, Kitagawa S. Selective guest sorption in an interdigitated porous framework with hydrophobic pore surfaces. Chem. Commun. 2007; 3395–3397. DOI:10.1039/B703502K

[52] Nakagawa K, Tanaka D, Horike S, Shimomura S, Higuchi M, Kitagawa S. Enhanced selectivity of CO2 from a ternary gas mixture in an interdigitated porous framework. Chem. Commun. 2010; 46:4258–4260. DOI:10.1039/C0CC00027B

[53] Loiseau T, Serre C, Huguenard C, Fink G, Taulelle F, Henry M, Bataille T, Ferey G. A rationale for the large breathing of the porous aluminum terephthalate (MIL-53) upon hydration. Chem. Eur. J. 2004; 10:1373–1382. DOI:10.1002/chem.200305413

[54] Horcajada P, Serre C, Maurin G, Ramsahye NA, Balas F, Vallet-Regi M, Sebban M, Taulelle F, Ferey G. Flexible porous metal-organic frameworks for a controlled drug delivery. J. Am. Chem. Soc. 2008; 130:6774–6780. DOI:10.1021/ja710973k

[55] Finsy V, Kirschhock CEA, Vedts G, Maes M, Alaerts L, De Vos DE, Baron GV, Denayer JFM. Framework breathing in the vapour-phase adsorption and separation of xylene isomers with the metal–organic framework MIL-53. Chem. Eur. J. 2009; 15:7724–7731. DOI:10.1002/chem.200802672

[56] Barcia PS, Zapata F, Silva JAC, Rodrigues AE, Chen BL. Kinetic separation of hexane isomers by fixed-bed adsorption with a microporous metal–organic framework. J. Phys. Chem. B. 2007; 111:6101–6103. DOI:10.1021/jp0721898

[57] Kitagawa S, Kitaura R, Noro S. Functional porous coordination polymers. Angew. Chem. Int. Ed. 2004; 43:2334–2375. DOI:10.1002/anie.200300610

[58] Farha OK, Yazaydin AO, Eryazici I, Malliakas CD, Hauser BG, Kanatzidis MG, Nguyen ST, Snurr RQ, Hupp JT. De novo synthesis of a metal–organic framework material

featuring ultrahigh surface area and gas storage capacities. Nat. Chem. 2010; 2:944–948. DOI:10.1038/nchem.834

[59] Dinca M, Dailly A, Liu Y, Brown CM, Neumann DA, Long JR. Hydrogen storage in a microporous metal–organic framework with exposed Mn2+ coordination sites. J. Am. Chem. Soc. 2006; 128:16876–16883. DOI:10.1021/ja0656853

[60] Dinca M, Long JR. Hydrogen storage in microporous metal-organic frameworks with exposed metal sites. Angew. Chem. Int. Ed. 2008; 47:6766–6779. DOI:10.1002/anie.200801163

[61] Chen B, Ockwig NW, Millward AR, Contreras DS, Yaghi OM. High H2 adsorption in a microporous metal–organic framework with open metal sites. Angew. Chem., Int. Ed. 2005; 44:4745–4749. DOI:10.1002/anie.200462787

[62] Rowsell JLC, Yaghi OM. Strategies for hydrogen storage in metal-organic frameworks. Angew. Chem. Int. Ed. 2005; 44:4670–4679. DOI:10.1002/anie.200462786

[63] Jung DH, Kim D, Lee TB, Choi SB, Yoon JH, Kim J, Choi K, Choi SHJ. Grand canonical Monte Carlo simulation study on the catenation effect on hydrogen adsorption onto the interpenetrating metal−organic frameworks. Phys. Chem. B. 2006; 110:22987–22990. DOI:10.1021/jp065819z

[64] Ma S, Sun D, Ambrogio M, Fillinger JA, Parkin S, Zhou HC. Framework-catenation isomerism in metal−organic frameworks and its impact on hydrogen uptake. J. Am. Chem. Soc. 2007; 129:1858–1859. DOI:10.1021/ja067435s

[65] Ryan P, Broadbelt LJ, Snurr RQ. Is catenation beneficial for hydrogen storage in metal–organicframeworks? Chem. Commun. 2008; 4132–4134. DOI:10.1039/B804343D

[66] Han SS, Mendoza-Cortes JL, Goddard WA III. Recent advances on simulation and theory of hydrogen storage in metal–organic frameworks and covalent organic frameworks. Chem. Soc. Rev. 2009; 38:1460–1476. DOI:10.1039/B802430H

[67] Mulfort KL, Farha OK, Stern CL, Sarjeant AA, Hupp JT. Post-synthesis alkoxide formation within metal−organic framework materials: a strategy for incorporating highly coordinatively unsaturated metal ions. J. Am. Chem. Soc. 2009; 131:3866–3868. DOI:10.1021/ja809954r

[68] Himsl D, Wallacher D, Hartmann M. Improving the hydrogen-adsorption properties of a hydroxy-modified MIL-53(Al) structural analogue by lithium doping. Angew. Chem. Int. Ed. 2009; 48:4639–4642. DOI:10.1002/anie.200806203

[69] Murray LJ, Dinca M, Long JR. Hydrogen storage in metal–organic frameworks. Chem. Soc. Rev. 2009; 38:1294–1314. DOI:10.1039/B802256A

[70] Suh MP, Park HJ, Prasad TK, Lim DW. Hydrogen storage in metal–organic frameworks. Chem. Rev. 2012; 112:782–835. DOI:10.1021/cr200274s

[71] Burchell, T.; Rogers, M. Low pressure storage of natural gas for vehicular applications. SAE Tech. Pap. Ser. 2000; 2000-01-2205. DOI:10.4271/2000-01-2205

[72] Ma SQ, Sun DF, Simmons JM, Collier CD, Yuan DQ, Zhou HC. Metal-organic framework from an anthracene derivative containing nanoscopic cages exhibiting high methane uptake. J. Am. Chem. Soc. 2008; 130:1012–1016. DOI:10.1021/ja0771639

[73] Bhatia SK, Myers AL. Optimium conditions for adsorptive storage. Langmuir. 2006; 22:1688–1700. DOI:10.1021/la0523816

[74] Furukawa H, Miller MA, Yaghi OM. Independent verification of the saturation hydrogen uptake in MOF-177 and establishment of a benchmark for hydrogen adsorption in metal–organic frameworks. J. Mater. Chem. 2007; 17:3197–3204. DOI: 10.1039/B703608F

[75] P€assler P, Hefner W, Buckl K, Meinass H, Meiswinkel A, Wernicke, H-J, Ebersberg G, M€uller R, B€assler J, Behringer H, Mayer D. Acetylene; Wiley-VCH Verlag GmbH & Co. KGaA: New York, 2000.

[76] Xiang SC, Zhou W, Zhang ZJ, Green MA, Liu Y, Chen BL. Open metal sites within isostructural metal-organic frameworks for differential recognition of acetylene and extraordinarily high acetylene storage capacity at room temperature. Angew. Chem., Int. Ed. 2010; 49:4615–4618. DOI:10.1002/anie.201000094

[77] Zhang JP, Chen XM. Optimized acetylene/carbon dioxide sorption in a dynamic porous crystal. J. Am. Chem. Soc. 2009; 131:5516–5521. DOI:10.1021/ja8089872

[78] Hu YX, Xiang SC, Zhang WW, ZhangZX, Wang L, Bai JF, Chen BL. A new MOF-505 analog exhibiting high acetylene storage. Chem. Commun. 2009; 7551–7553. DOI: 10.1039/B917046D

[79] Rosi N, Kim J, Eddaouddi M, Chen B, O'Keeffe M, Yaghi OM. Rod packings and metal −organic frameworks constructed from rod-shaped secondary building units. J. Am. Chem. Soc. 2005; 127:1504–1518. DOI:10.1021/ja045123o

[80] Dietzel PDC, Besikiotis V, Blom R. Application of metal–organic frameworks with coordinatively unsaturated metal sites in storage and separation of methane and carbon dioxide. J. Mater. Chem. 2009; 19:7362–7370. DOI:10.1039/B911242A

[81] Cundy CS, Cox PA. The hydrothermal synthesis of zeolites: history and development from the earliest days to the present time. Chem. Rev. 2003; 103:663–702. DOI: 10.1021/cr020060i

[82] Stock N, Biswas S. Synthesis of metal-organic frameworks (MOFs): routes to various MOF topologies, morphologies, and composites. Chem. Rev. 2012; 112:933–969. DOI: 10.1021/cr200304e

[83] Bauer S, Serre C, Devic T, Horcajada P, Marrot J, Férey G, Stock N. High-throughput assisted rationalization of the formation of metal organic frameworks in the iron(III)

aminoterephthalate solvothermal system. Inorg. Chem. 2008; 47:7568–7576. DOI: 10.1021/ic800538r

[84] Khan NA, Kang IJ, Seok HY, Jhung SH. Facile synthesis of nano-sized metal-organic frameworks, chromium-benzenedicarboxylate, MIL-101. Chem. Eng. J. 2011; 166:1152–1157. DOI:10.1016/j.cej.2010.11.098

[85] Zhao Z, Li X, Huang S, Xia Q, Li Z. Adsorption and diffusion of benzene on chromium-based metal organic framework MIL-101 synthesized by microwave irradiation. Ind. Eng. Chem. Res. 2011; 50:2254–2261. DOI:10.1021/ie101414n

[86] Choi JY, Kim J, Jhung SH, Kim HK, Chang J-S, Chae HK. Microwave synthesis of a porous metal-organic framework, zinc terephthalate MOF-5. Bull. Korean Chem. Soc. 2006; 27:1523–1524. DOI:10.5012/bkcs.2006.27.10.1523

[87] Ren J, Langmi HW, North BC, Mathe M, Bessarabov D. Modulated synthesis of zirconium-metal organic framework (Zr-MOF) for hydrogen storage applications. Int. J. Hydrogen Energy. 2014; 39:890–895. DOI:10.1016/j.ijhydene.2013.10.087

[88] Liang W, D'Alessandro DM. Microwave-assisted solvothermal synthesis of zirconium oxide based metal-organic frameworks. Chem. Commun. 2013; 49:3706–3708. DOI:10.1039/c3cc40368h.

[89] Ren J, Segakweng T, Langmi H, Musyoka N, North B, Mathe M, Bessarabov D. Microwave-assisted modulated synthesis of zirconium-based metal–organic framework (Zr-MOF) for hydrogen storage applications. Int. J. Mater. Res. 2014; 105:516–519. DOI:10.3139/146.111047

[90] Wu RF, Zhang TL, Qiao XJ, Zhang JG, Liu YH. Synthesis, crystal structure and thermal stability of a novel 3D coordination polymer Pb(1,4-napdc)(DMF). Chin. J. Inorg. Chem. 2006; 22:1340–1344. ISSN: 1001-4861; 22(7).

[91] Tuikka M, Haukka M, Ahlgrén M. Three barium diphosphonates with 3-D structures. Solid State Sci. 2007; 9:535–541. DOI:10.1016/j.solidstatesciences.2007.04.006

[92] Yuan W, O'Connor J, James SL. Mechanochemical synthesis of homo- and hetero-rare-earth(III) metal–organic frameworks by ball milling. CrystEngComm. 2010; 12:3515–3517. DOI:10.1039/C0CE00216J

[93] Seoane B, Zamaro JM, Tellez C, Coronas J. Sonocrystallization of zeolitic imidazolate frameworks (ZIF-7, ZIF-8, ZIF-11 and ZIF-20). CrystEngComm. 2012; 14:3103–3107. DOI:10.1039/C2CE06382D

[94] Thompson JA, Chapman KW, Koros WJ, Jones CW, Nair S. Sonication-induced Ostwald ripening of ZIF-8 nanoparticles and formation of ZIF-8/polymer composite membranes. Microporous Mesoporous Mater. 2012; 158:292–299. DOI:10.1016/j.micromeso.2012.03.052

[95] Bang JH, Suslick KS. Applications of ultrasound to the synthesis of nanostructured materials. Adv. Mater. 2010; 22:1039–1059. DOI:10.1002/adma.200904093

[96] Tranchemontagne DJ, Hunt JR, Yaghi OM. Room temperature synthesis of metal-organic frameworks: MOF-5, MOF-74, MOF-177, MOF-199, and IR MOF-0. Tetrahedron. 2008; 64:8553–8557. DOI:10.1016/j.tet.2008.06.036

[97] Schlesinger M, Schulze S, Hietschold M, Mehring M. Evaluation of synthetic methods for microporous metal–organic frameworks exemplified by the competitive formation of [Cu2(btc)3(H2O)3] and [Cu2(btc)(OH)(H2O)]. Microporous Mesoporous Mater. 2010; 132:121–127. DOI:10.1016/j.micromeso.2010.02.008

[98] Fard MJS, Rastaghi F, Ghanbari N. Sonochemical synthesis of new nano-two-dimensional lead(II) coordination polymer: as precursor for preparation of PbO nanostructure. J. Mol. Struct. 2013; 1032:133–137. DOI:10.1016/j.molstruc.2012.07.020

[99] Martinez Joaristi A, Juan-Alcaniz J, Serra-Crespo P, Kapteijn F, Gascon J. Electrochemical synthesis of some archetypical Zn2+, Cu2+, and Al3+ metal organic framework. Cryst. Growth Des. 2012; 12:3489–3498. DOI:10.1021/cg300552w

[100] Campagnol N, Van Assche T, Boudewijns T, Denayer J, Binnemans K, De Vos D, Fransaer J. High pressure, high temperature electrochemical synthesis of metal–organic frameworks: films of MIL-100 (Fe) and HKUST-1 in different morphologies. J. Mater. Chem. A. 2013; 1:5827–5830. DOI:10.1039/C3TA10419B

[101] Stassen I, Styles M, Van Assche T, Campagnol N, Fransaer J, Denayer J, Tan J-C, Falcaro P, De Vos D, Ameloot R. Electrochemical film deposition of the zirconium metal–organic framework UiO-66 and application in a miniaturized sorbent trap. Chem. Mater. 2015; 27:1801–1807. DOI:10.1021/cm504806p

[102] Youngblood WJ, Lee SA, Kobayashi Y, Hernandez-Pagan E, Hoertz PG, Moore TA, Moore AL, Gust D, Mallouk TE. Photoassisted overall water splitting in a visible light-absorbing dye-sensitized photoelectrochemical cell. J. Am. Chem. Soc. 2009; 131:926–927. DOI:10.1021/ja809108y

[103] Reece SY, Hamel JA, Sung K, Jarvi TD, Esswein AJ, Pijpers JJH, Nocera DG. Wireless solar water splitting using silicon-based semiconductors and earth-abundant catalysts. Science. 2011; 334:645–648. DOI:10.1126/science.1209816

[104] Ohno T, Bai L, Hisatomi T, Maeda K, Domen K. Photocatalytic water splitting using modified GaN:ZnO solid solution under visible light: long-time operation and regeneration of activity. J. Am. Chem. Soc. 2012; 134:8254–8259. DOI:10.1021/ja302479f

[105] Wang X, Xu Q, Li M, Shen S, Wang X, Wang Y, Feng Z, Shi J, Han H, Li C. Photocatalytic overall water splitting promoted by an phase junction on Ga2O3. Angew. Chem. Int. Ed. 2012; 51:13089–13092. DOI:10.1002/anie.201207554

[106] Nicewicz DA, MacMillan DWC. Merging photo redox catalysis with organo catalysis: the direct asymmetric alkylation of aldehydes. Science. 2008; 322:77–80. DOI:10.1126/science.1161976

[107] Nagib DA, Scott ME, MacMillan DWC. Enantioselective α-trifluoromethylation of aldehydes via photoredox organo catalysis. J. Am. Chem. Soc. 2009; 131:10875–10877. DOI:10.1021/ja9053338

[108] Du J, Yoon TP. Crossed intermolecular [2+2] cycloadditions of acyclic enones via visible light photocatalysis. J. Am. Chem. Soc. 2009; 131:14604–14605.

[109] Condie AG, Gonza ´lez-Go ´mez JC, Stephenson CRJ. Visible-light photoredox catalysis: Aza-Henry reactions via C-H functionalization. J. Am. Chem. Soc. 2010; 132:1464–1465.

[110] Lang X, Ji H, Chen C, Ma W, Zhao J. Selective formation of imines by aerobic photocatalytic oxidation of amines on TiO2. Angew. Chem. Int. Ed. 2011; 50:3934–3937

[111] Chen W, Rein FN, Rocha RC. Homogeneous photocatalytic oxidation of alcohols by a chromophore-catalyst dyad of ruthenium complexes. Angew. Chem. Int. Ed. 2009; 48:9672–9675. DOI:10.1002/anie.200904756

[112] Li F, Jiang Y, Zhang B, Huang F, Gao Y, Sun L. Towards a solar fuel device: light-driven water oxidation catalyzed by a supramolecular assembly. Angew. Chem. Int. Ed. 2012; 51:2417–2420. DOI:10.1002/anie.201108051

[113] Windle CD, Perutz RN. Advances in molecular photocatalytic and electrocatalytic CO2 reduction. Coord. Chem. Rev. 2012; 256:2562–2570. DOI:10.1016/j.ccr.2012.03.010

[114] Yoon M, Srirambalaji R, Kim K. Homochiral metal–organic frameworks for asymmetric heterogeneous catalysis. Chem. Rev. 2012; 112:1196–1231. DOI:10.1021/cr2003147

[115] Cavka JH, Jakobsen S, Olsbye U, Guillou N, Lamberti C, Bordiga S, Lillerud KP. A new zirconium inorganic building brick forming metal organic frameworks with exceptional stability. J. Am. Chem. Soc. 2008; 130:13850–13851. DOI:10.1021/ja8057953

[116] Gomes Silva C, Luz I, Llabre ´s i Xamena FX, Corma A, Garcı ´a H. Water stable Zr–benzenedicarboxylate metal–organic frameworks as photocatalysts for hydrogen generation. Chem. Eur. J. 2010; 16:11133–11138. DOI:10.1002/chem.200903526

[117] Sun D, Fu Y, Liu W, Ye L, Wang D, Yang L, Fu X, Li Z. Studies on photocatalytic CO2 reduction over NH2-Uio-66(Zr) and its derivatives: towards a better understanding of photocatalysis on metal–organic frameworks. Chem. Eur. J. 2013; 19:14279–14285. DOI:10.1002/chem.201301728

[118] Wang C, deKrafft KE, Lin W. Pt nanoparticles@photoactive metal-organic frameworks: efficient hydrogen evolution via synergistic photoexcitation and electron injection. J. Am. Chem. Soc. 2012; 134:7211–7214. DOI:10.1021/ja300539p

[119] Hawecker J, Lehn J, Ziessel R. Efficient photochemical reduction of CO2 to CO by visible light irradiation of systems containing Re(bipy)(CO)3X or Ru(bipy)32+-Co2+ combi-

nations as homogeneous catalysts. J. Chem. Soc. Chem. Commun. 1983; 0:536–538. DOI:10.1039/C39830000536

[120] Lin W, Frei H. Photochemical CO2 splitting by metal-to-metal charge-transfer excitation in mesoporous ZrCu(I)-MCM-41 silicate sieve. J. Am. Chem. Soc. 2005; 127:1610–1611.

[121] Liu Q, Zhou Y, Kou J, Chen X, Tian Z, Gao J, Yan S, Zou Z. High-yield synthesis of ultra-long and ultrathin Zn2GeO4 nanoribbons toward improved photocatalytic reduction of CO2 into renewable hydrocarbon fuel. J. Am. Chem. Soc. 2010; 132:14385–14387.

[122] Yan S, Ouyang S, Gao J, Yang M, Feng J, Fan X, Wan L, Li Z, Ye J, Zhou Y, Zou Z. A room-temperature reactive-template route to mesoporous ZnGa2O4 with improved photocatalytic activity in reduction of CO2. Angew. Chem. Int. Ed. 2010; 49:6400–6404

[123] Wang C, Xie Z, DeKrafft KE, Lin W. Doping metal–organic frameworks for water oxidation, carbon dioxide reduction, and organic photocatalysis. J. Am. Chem. Soc. 2011; 133:13445–13454. DOI:10.1021/ja203564w

[124] Pullen S, Fei H, Orthaber A, Cohen SM, Ott S. Enhanced photochemical hydrogen production by a molecular diiron catalyst incorporated into a metal–organic framework. J. Am. Chem. Soc. 2013; 135:16997–17003. DOI:10.1021/ja407176p

[125] Wang JL, Wang C, Lin W. Metal-organic frameworks for light harvesting and photocatalysis. ACS Catalysis 2012; 2, 2630–2640, DOI:10.1021/cs3005874

[126] Navarro Amador R, Carboni M, Meyer D. Photosensitive titanium and zirconium metal organic frameworks: current research and future possibilities. Mater. Lett. 2015. DOI: 10.1016/j.matlet.2015.12.023

[127] Horiuchi Y, Toyao T, Takeuchi M, Matsuoka M, Anpo M. Recent advances in visible-light-responsive photocatalysts for hydrogen production and solar energy conversion-from semiconducting TiO2 to MOF/PCP photocatalysts. Phys. Chem. Chem. Phys. 2013; 15:13243–13253. DOI:10.1039/c3cp51427g

[128] Wang C-C, Li J-R, Lv X-L, Zhang Y-Q, Guo G. Photocatalytic organic pollutants degradation in metal-organic frameworks. Energy Environ. Sci. 2014; 7:2831–2867. DOI:10.1039/C4EE01299B

[129] Mahata P, Madras G, Natarajan S. Novel photocatalysts for the decomposition of organic dyes based on metal-organic framework compounds. J. Phys. Chem. B 2006; 110:13759–13768. DOI:10.1021/jp0622381

[130] Wang Y. et al. Controlled fabrication and enhanced visible-light photocatalytic hydrogen production of Au at CdS/MIL-101 heterostructure. Appl. Catalysis B Environ. 2016; 185:307–314. DOI:10.1016/j.apcatb.2015.12.020

[131] Sun D, Ye L, Li Z. Visible-light-assisted aerobic photocatalytic oxidation of amines to imines over NH2-MIL-125(Ti). Appl. Catalysis B Environ. 2015; 164:428–432. DOI: 10.1016/j.apcatb.2014.09.054

[132] Ke F, Wang L, Zhu J. Facile fabrication of CdS-metal-organic framework nanocomposites with enhanced visible-light photocatalytic activity for organic transformation. Nano Res. 2015; 8:1834–1846. DOI:10.1007/s12274-014-0690-x

[133] Kumar Paul A, Madras G, Natarajan S. Adsorption-desorption and photocatalytic properties of inorganic-organic hybrid cadmium thiosulfate compounds. Phys. Chem. Chem. Phys. 2009; 11:11285–11296. DOI:10.1039/B913407G

[134] Maeda K, Domen K. New non-oxide photocatalysts designed for overall water splitting under visible light. J. Phys. Chem. C 2007; 111:7851–7861. DOI:10.1021/jp070911w

[135] Gu Z. et al. Synthesis of Au@UiO-66(NH2) structures by small molecule-assisted nucleation for plasmon-enhanced photocatalytic activity. Chem. Commun. 2016; 52:116–119. DOI:10.1039/c5cc07042b

[136] Sun D, et al. Noble metals can have different effects on photocatalysis over metal-organic frameworks (MOFs): a case study on M/NH2-MIL-125(Ti) (M=Pt and Au). Chem. Eur. J. 2014; 20:4780–4788. DOI:10.1002/chem.201304067

[137] Liang R, et al. A simple strategy for fabrication of Pd@MIL-100(Fe) nanocomposite as a visible-light-driven photocatalyst for the treatment of pharmaceuticals and personal care products (PPCPs). Appl. Catalysis B Environ. 2015; 176–177, 240–248. DOI: 10.1016/j.apcatb.2015.04.009

[138] Tilgner D, Friedrich M, Hermannsdörfer J, Kempe R. Titanium dioxide reinforced metal-organic framework Pd catalysts: activity and reusability enhancement in alcohol dehydrogenation reactions and improved photocatalytic performance. ChemCatChem 2015; 7:3916–3922. DOI:10.1002/cctc.201500747

[139] Alvaro M, Carbonell E, Ferrer B, Llabrés i Xamena FX, Garcia H. Semiconductor behavior of a metal-organic framework (MOF). Chem. Eur. J. 2007; 13:5106–5112. DOI:10.1002/chem.200601003

[140] Llabrés i Xamena FX, Corma A, Garcia H. Applications for metal-organic frameworks (MOFs) as quantum dot semiconductors. J. Phys. Chem. C 2007; 111:80–85. DOI:10.1021/jp063600e

[141] Wen L-L, et al. Structures, photoluminescence, and photocatalytic properties of six new metal–organic frameworks based on aromatic polycarboxylate acids and rigid imidazole-based synthons. Crystal Growth Des. 2009; 9:3581–3589. DOI:10.1021/cg900317d

[142] Yu Z-T, Liao Z-L, Jiang Y-S, Li G-H, Chen J-S. Water-insoluble Ag–U–organic assemblies with photocatalytic activity. Chem. Eur. J. 2005; 11:2642–2650. DOI:10.1002/chem.200401189

[143] Yang LM, Pushpa R. Tuning electronic and optical properties of a new class of covalent organic frameworks. J. Mater. Chem. C 2014; 2:2404–2416. DOI:10.1039/c3tc32252a

[144] Yang L-M, Fang G-Y, Ma J, Ganz E, Han SS. Band gap engineering of paradigm MOF-5. Crystal Growth Des. 2014; 14:2532–2541. DOI:10.1021/cg500243s

[145] Zhang H, Zhou Y, Song X. Advanced functional materials derived from metal-organic frameworks. Prog. Chem. 2015; 27:174–191. DOI:10.7536/PC140925

[146] Odoh SO, Cramer CJ, Truhlar DG, Gagliardi L. Quantum-chemical characterization of the properties and reactivities of metal–organic frameworks. Chem. Rev. 2015; 115:6051–6111. DOI:10.1021/cr500551h

[147] Shen L, et al. Noble-metal-free MoS2 co-catalyst decorated UiO-66/CdS hybrids for efficient photocatalytic H2 production. Appl. Catalysis B Environ. 2015; 166–167, 445–453. DOI:10.1016/j.apcatb.2014.11.056

[148] Gao ST, et al. Integration of a plasmonic semiconductor with a metal-organic framework: a case of Ag/AgCl@ZIF-8 with enhanced visible light photocatalytic activity. RSC Adv. 2014; 4:61736–61742. DOI:10.1039/c4ra11364k

[149] Xie MH, Yang XL, Zou C, Wu CD. A Sn IV-porphyrin-based metal-organic framework for the selective photo-oxygenation of phenol and sulfides. Inorg. Chem. 2011; 50:5318–5320, DOI:10.1021/ic200295h

[150] Zhan W-w, et al. Semiconductor@Metal–organic framework core–shell heterostructures: a case of ZnO@ZIF-8 nanorods with selective photoelectrochemical response. J. Am. Chem. Soc. 2013; 135:1926–1933. DOI:10.1021/ja311085e

[151] Lee DY. Cu-based metal–organic frameworks for photovoltaic application. J. Phys. Chem. C 2014; 118:16328–16334. DOI:10.1021/jp4079663

[152] Lee DY. Layer-by-layer deposition and photovoltaic property of Ru-based metal-organic frameworks. RSC Adv. 2014; 4:12037–12042. DOI:10.1039/C4RA00397G

[153] Shi L. An amine-functionalized iron(III) metal–organic framework as efficient visible-light photocatalyst for Cr(VI) reduction. Adv. Sci. 2015; 2:n/a–n/a. DOI:10.1002/advs.201500006

[154] Shen L, Wu W, Liang R, Lin R, Wu L. Highly dispersed palladium nanoparticles anchored on UiO-66(NH2) metal-organic framework as a reusable and dual functional visible-light-driven photocatalyst. Nanoscale 2013; 5:9374–9382. DOI:10.1039/c3nr03153e

[155] Shen L, Wu W, Liang R, Lin R, Wu L. Highly dispersed palladium nanoparticles anchored on UiO-66(NH2) metal-organic framework as a reusable and dual functional visible-light-driven photocatalyst. Nanoscale. 2013; 5(19):9374–82. DOI:10.1039/c3nr03153e

INTECH